Biogeosciences Discuss., 12, 19213–19267, 2015
www.biogeosciences-discuss.net/12/19213/2015/
doi:10.5194/bgd-12-19213-2015

Biogeosciences
Discussions
Open Access

MODIS vegetation products as proxies of photosynthetic potential: a look across meteorological and biologic driven ecosystem productivity

N. Restrepo-Coupe[1], A. Huete[1], K. Davies[1,7], J. Cleverly[2,8], J. Beringer[3], D. Eamus[2,8], E. van Gorsel[4], L. B. Hutley[5], and W. S. Meyer[6]

[1]Plant Functional Biology and Climate Change Cluster, University of Technology Sydney, P.O. Box 123, Broadway, NSW, 2007, Australia
[2]School of Life Sciences, University of Technology Sydney, P.O. Box 123, Broadway, NSW, 2007, Australia
[3]School of Earth and Environment, The University of Western Australia, Crawley, WA, 6009, Australia
[4]CSIRO Oceans and Atmosphere, Forestry House, Building 002, Wilf Crane Crescent, Yarralumla, ACT 2601, Australia
[5]Research Institute for the Environment and Livelihoods, Charles Darwin University, Darwin, NT 0909, Australia
[6]Environment Institute, School of Biological Sciences, University of Adelaide, Adelaide, SA, 5005, Australia

[7]School of Geosciences, University of Sydney NSW 2006, Australia
[8]Australian SuperSite Network

Received: 28 August 2015 – Accepted: 2 November 2015 – Published: 4 December 2015

Correspondence to: N. Restrepo-Coupe (nataliacoupe@gmail.com)
and A. Huete (alfredo.huete@uts.edu.au)

Published by Copernicus Publications on behalf of the European Geosciences Union.

Abstract

A direct relationship between gross ecosystem productivity (GEP) measured by the eddy covariance (EC) method and Moderate Resolution Imaging Spectroradiometer (MODIS) vegetation indices (VIs) has been observed in many temperate and tropical ecosystems. However, in Australian evergreen forests, and particularly sclerophyll woodlands, MODIS VIs do not capture seasonality of GEP. In this study, we re-evaluate the connection between satellite and flux tower data at four contrasting Australian ecosystems, through comparisons of ecosystem photosynthetic activity (GEP) and potential (e.g. ecosystem light use efficiency and quantum yield) with MODIS vegetation satellite products, including VIs, gross primary productivity ($\mathrm{GPP_{MOD}}$), leaf area index ($\mathrm{LAI_{MOD}}$), and fraction of photosynthetic active radiation ($\mathrm{fPAR_{MOD}}$). We found that satellite derived greenness products constitute a measurement of ecosystem structure (e.g. leaf area index – quantity of leaves) and function (e.g. leaf level photosynthetic assimilation capacity – quality of leaves), rather than productivity. Our results show that in primarily meteorological-driven (e.g. photosynthetic active radiation, air temperature and/or precipitation) and relatively aseasonal vegetation photosynthetic potential ecosystems (e.g. evergreen wet sclerophyll forests), there were no statistically significant relationships between GEP and satellite derived measures of greenness. In contrast, for phenology-driven ecosystems (e.g. tropical savannas), changes in the vegetation status drove GEP, and tower-based measurements of photosynthetic activity were best represented by VIs. We observed the highest correlations between MODIS products and GEP in locations where key meteorological variables and vegetation phenology were synchronous (e.g. semi-arid *Acacia* woodlands) and low correlation at locations where they were asynchronous (e.g. Mediterranean ecosystems). Eddy covariance data offer much more than validation and/or calibration of satellite data and models. Knowledge of the conditions in which flux tower measurements and VIs or other remote sensing products converge greatly advances our understanding of

the mechanisms driving the carbon cycle (phenology and climate drivers) and provides an ecological basis for interpretation of satellite derived measures of greenness.

1 Introduction

Eddy flux towers constitute a powerful tool to measure and study carbon, energy and water fluxes. Even though the number of eddy covariance (EC) sites has been steadily increasing (Baldocchi, 2014; Baldocchi et al., 2001), instrumentation, personnel costs, and equipment maintenance, limit the establishment of new sites. This is demonstrated by the distribution of flux towers around the world and in particular the underrepresentation of tropical and semi-arid locations in the Southern Hemisphere (Australia, Africa, and South America; http://fluxnet.ornl.gov/maps-graphics and Beringer et al., 2007). The first EC tower was established in 1990 at Harvard Forest (Wofsy et al., 1993) followed by five other sites in 1993 (Baldocchi, 2003). In Australia, only two locations, Howard Springs (Hutley et al., 2000) and Tumbarumba (Van Gorsel et al., 2013), have a record that extends more than 10 years.

Many applications rely on large-scale, remotely sensed (RS) representations of vegetation dynamics (greenness) to: (1) up-scale water and carbon fluxes from the limited tower footprint (radius < 10 km) representative of eddy covariance measurements, (2) scale fluxes in time and extend a longer time series from limited tower data, (3) fill gaps due to quality control in the flux measurements, (4) study continental phenology to be validated at flux tower sites, and (5) parameterise land surface and agricultural models to be tested at EC locations. Where satellite derived greenness indices (VIs) represent a community property of chlorophyll content, leaf area index (LAI), and fractional vegetation cover; past studies have focused on the relationship between the Moderate Resolution Imaging Spectroradiometer, (MODIS) VIs, such as the enhanced vegetation index (EVI), and tower based measurements of gross ecosystem productivity (GEP; Gamon et al., 2013; Huete et al., 2008, 2006; Maeda et al., 2014; Sims et al., 2006; Wang et al., 2004). A simple linear regression between seasonal (monthly or 16-day) EVI and GEP has previously provided a good coefficient of determination (R^2) for different ecosystems:

$$\text{GEP} = b_0 + b_1 \times \text{EVI} \tag{1}$$

where b_0 and b_1 are the fitted coefficients. Huete et al. (2006) reported an R^2 of 0.5 for Eq. (1) in tropical forests and converted pastures over the Amazon basin, and an R^2 of 0.74 in dry to humid tropical forest sites in Southeast Asia (Huete et al., 2008). Over the North Australian mesic and xeric tropical savannas, R^2 ranged from 0.52 at a wooded grassland (Alice Springs, ASP) to 0.89 in woodlands (Howard Springs, HSP; Ma et al., 2013).

Similar relationships to Eq. (1) have been explored using monthly maximal net ecosystem exchange (NEE_{max}):

$$\text{NEE}_{\text{max}} = b_0 + b_1 \times \text{EVI} \tag{2}$$

This regression showed an improved fit in forests ($R^2 = 0.83$ for deciduous and $R^2 = 0.72$ for coniferous forests) compared to the GEP-EVI model ($R^2 = 0.81$ for deciduous and $R^2 = 0.69$ for evergreen forests; Olofsson et al., 2008).

Other approaches to link carbon fluxes to RS products include radiation–greenness (R–G) models, where both a meteorological driver, represented by the photosynthetic active radiation (PAR), and a vegetation phenology driver, represented by EVI or by the normalized difference vegetation index (NDVI), are implicitly included in the model (Ma et al., 2014; Peng and Gitelson, 2012). By definition, the GEP/PAR ratio is commonly referred as ecosystem light use efficiency (LUE), where:

$$\text{LUE} = b_0 + b_1 \times \text{EVI} \tag{3}$$

However, the EVI vs. LUE relationship has shown lower R^2 values (0.76) compared to the EVI vs. GEP regression (0.92) for a group of North American ecosystems that included evergreen needleleaf and deciduous forests, grasslands and savannas (Sims et al., 2006). Hill et al. (2006) also reported an R^2 of ~ 0.2 for the NDVI vs. LUE relationship for the Australian sclerophyll forest of Tumbarumba, however, the result was not statistically significant ($p > 0.05$). To better represent GEP at rainfall-driven semi-arid ecosystems, Sjöström et al. (2011) increased the level of complexity of the R–G model by scaling down observations of PAR using the evaporative fraction (EF) term from EC measurements (a proxy for water availability), thus GEP was calculated as:

$$\mathrm{GEP} = \mathrm{EVI} \times \mathrm{PAR} \times \mathrm{EF} \tag{4}$$

where EF is the ratio between latent heat flux (LE) and the surface turbulent fluxes ($H + \mathrm{LE}$), and H is defined as the sensible heat flux, $\mathrm{EF} = \mathrm{LE}/(H + \mathrm{LE})$. The model increased the predictive power of the R–G model in some ecosystems; however, it was not applicable at regional scales due to its reliance upon supporting tower measurements.

Temperature–greenness models (T–G) use the MODIS Land Surface Temperature product (LST) and VIs to calculate GEP as in Sims et al. (2008). The T–G GEP model for nine North American temperate EC sites was calculated as:

$$\mathrm{GEP} = \mathrm{EVI}_{\mathrm{scaled}} \times \mathrm{LST}_{\mathrm{scaled}} \times m \tag{5}$$

where m is a function of mean annual LST and plant functional type (different formulation provided for evergreen and deciduous vegetation), $\mathrm{LST}_{\mathrm{scaled}}$ is the minimum of two equations ($\mathrm{LST}/30$) and ($2.5 - (0.05 \times \mathrm{LST})$), and $\mathrm{EVI}_{\mathrm{scaled}}$ is $\mathrm{EVI} - 0.10$. A similar T–G model, used by Wu et al. (2011), showed high correlation at deciduous forests ($R^2 = \sim 0.90$) and lower R^2 values at non-forest areas ($R^2 = 0.27$ to 0.91) and evergreen forests ($R^2 = 0.28$ to 0.91).

Other more complex derivations, including the C-Fix model (Veroustraete et al., 2002) and the MODIS Gross Primary Productivity product ($\mathrm{GPP}_{\mathrm{MOD}}$), rely on biome specific relationships that include: (1) vegetation phenology represented by MODIS derived fraction of absorbed PAR that a plant canopy absorbs for photosynthesis and growth ($\mathrm{fPAR_{MOD}}$); and (2) air temperature (T_{air}), water vapour pressure deficit (VPD), and PAR as climate drivers (Running et al., 2000). When applied to Australian ecosystems, the $\mathrm{GPP_{MOD}}$ (collection 4) was able to estimate the amplitude of the GEP annual cycle in a temperate evergreen wet sclerophyll forest (*Eucalyptus* dominated), however, it was out-of-phase (Leuning et al., 2005). For a tropical savanna (HSP), $\mathrm{GPP_{MOD}}$ (collection 5) overestimated dry season GEP (Kanniah et al., 2009). Even though, $\mathrm{GPP_{MOD}}$ (collection 4.8) at HSP accurately represented seasonality in productivity; low estimates of PAR and other model input variables were compensated by abnormally high $\mathrm{fPAR_{MOD}}$ values (Kanniah et al., 2009). A clear indication of obtaining a good result for the wrong reasons.

Besides the difficulties inherent in determining GEP in diverse ecosystems, all of the complex models (e.g. $\mathrm{GPP_{MOD}}$ and T–G model) require in situ measurements of water fluxes, PAR, and/or biome classification information to calibrate or derive some variables and consequently, regression coefficients do not necessarily extend to ecosystem types other than those for which the derivation was obtained. In this work, we revisit the GEP vs. EVI, and GEP vs. $\mathrm{GPP_{MOD}}$ regressions at different sites. Rather than attempting to determine the "best performing model", our first objective was to gain an understanding of ecosystem behaviour. We look at particularly challenging land cover classes: seasonal wet-dry and xeric tropical savannas, Mediterranean environments characterized by hot and dry summers (Mallee), and temperate evergreen sclerophyll forests. The selected locations are part of the OzFlux eddy-covariance network and represent sites where previous studies have shown satellite derived GEP models to be unable to replicate in situ measurements.

Our second objective was to derive and explore the seasonality of the different ground-based measures of vegetation photosynthetic potential: quantum yield (α), photosynthetic capacity (Pc), GEP at saturation light ($\mathrm{GEP_{sat}}$), and ecosystem light use efficiency (LUE) in an attempt to separate the vegetation structure and function (phenology) from the climatic drivers of productivity. We aimed to determine if EVI was able to replicate absolute value and seasonality of photosynthetic potential (α, Pc, LUE,

GEP_{sat}) rather than photosynthetic activity (GEP), based on linear regressions. Similarly, we included in our analysis other MODIS biophysical datasets (NDVI, LAI_{MOD}, and $fPAR_{MOD}$) in an effort to understand how to interpret different satellite measures of greenness and how these products can inform modellers and ecologists about vegetation phenology. In contrast to biome-specific classification approaches, we treated the relationship between greenness and photosynthetic potential to be a continuum and therefore, we explored multiple site regressions.

Finally, we combined satellite-derived meteorology (radiation, precipitation and temperature) and biological drivers (vegetation phenology) to determine site specific and multi-biome GEP values using multiple regression models. In this study, we evaluated the advantages of introducing both types of variables; we determine if the regressions hold across biomes, and whether productivity processes are driven by phenology, light, water availability and temperature; and we infer which of these variables govern the GEP seasonal cycle for each particular ecosystem. These results advance our understanding of driving mechanisms of the carbon cycle (climate, biological adaptation, or a combination of both), temporal and spatial scaling, and provide an ecological basis for the interpretation of satellite derived measures of greenness and phenology products.

2 Methods

2.1 Study sites

The OzFlux infrastructure network is operated by a collaborative research group and was set up to provide the Australian and global ecosystem modelling communities with CO_2 and H_2O flux and meteorological data (Beringer et al., 2015). We selected four contrasting long-term eddy flux (EC) sites from the OzFlux network (Fig. 1 and Table 1) for this study.

In northern Australia the Howard Springs (HSP) eddy flux tower is located in the Black Jungle Conservation Reserve, an open woodland savanna dominated by an understory of annual grasses and two overstory tree species: *Eucalyptus miniata* and *Eucalyptus tentrodonata* (Hutley et al., 2011; Kanniah et al., 2011). In the middle of the continent, among the xeric tropical savannas, the Alice Springs Mulga site (ASP) is located in a semi-arid Mulga woodland dominated by *Acacia aneura* and different annual and perennial grasses including Mitchell Grass (gen. *Astrebla*) and Spinifex (gen. *Triodia*; Cleverly et al., 2013; Eamus et al., 2013). Classified as a Mediterranean environment and characterized by hot and dry summers, the Calperum–Chowilla flux tower (CHO), is located at the fringes of the River Murray floodplains, a Mallee site (multi-stemmed *Eucalyptus socialis* and *E. dumosa* open woodland; Meyer et al., 2015). The evergreen Tumbarumba (TBR) site is located in Bago State Forest, NSW and classified as temperate evergreen wet sclerophyll (hard-indigestible leaves) forest. It is dominated by 40 m tall *Eucalyptus delegatensis* trees (Leuning et al., 2005; van Niel et al., 2012).

Fluxes at all towers were measured by the EC method with an open-path system. Simultaneously, an array of different sensors measured meteorological data including air temperature (T_{air}), relative humidity (RH), incoming and reflected short wave radiation (SW_{down} and SW_{up}), and incoming and reflected long wave radiation (LW_{down} and LW_{up}). Refer to each site references for complete information regarding ecosystem and measurement techniques.

2.2 Eddy covariance data

We used Level 3 OzFlux data that includes an initial OzFlux standard quality control (QA; Isaac et al., 2015). All data were subject to the same quality assurance procedures and calculations, providing methodological consistency among sites and reducing the uncertainty of the calculated fluxes. We performed additional quality checks and removal of outliers, and data were corrected for low turbulence periods (see Sect. 2.2.1). Ecosystem respiration (R_{eco}) and GEP were calculated from EC measurements of net ecosystem exchange (NEE) as presented in Sect. 2.2.2. Finally, we derived different measures of ecosystem vegetation photosynthetic potential (Sect. 2.2.3).

2.2.1 Eddy covariance and meteorological measurements

Incoming and outgoing radiation, both shortwave (SW_{down}, and SW_{up}) and longwave (LW_{down} and LW_{up}), were measured using a CNR1 Net Radiometer instrument (Campbell Scientific). All sensors were placed above the canopy at the same height or higher than the EC system. As there were no measurements of PAR radiation available at ASP, TBR and CHO, we assumed $\mathrm{PAR} = 2 \times \mathrm{SW}$ (Papaioannou et al., 1993; Szeicz, 1974), where PAR is measured as flux of photons ($\mu\mathrm{mol\,m^{-2}\,s^{-1}}$) and SW_{down} as heat flux density ($\mathrm{W\,m^{-2}}$). We understood this as an approximation because PAR radiation (0.4–0.7 nm) is a spectral subset of SW_{down} (0.3–3 nm).

At TBR, the NEE is calculated as the sum of the turbulent flux measured by eddy covariance (F_C) plus changes in the amount of CO_2 in the canopy air space (storage flux, S_{CO_2}), where $\mathrm{NEE} = F_C + S_{CO_2}$. At all other sites, given the sparse vegetation cover and the smaller control volume over the vegetation which is lower in height, F_C is assumed to be representative of NEE.

Hourly fluxes measured during rainy periods, when the sonic anemometer and the open path infrared gas analyser (IRGA) do not function correctly, were identified and removed from the time series. We also removed isolated observations (between missing values). We identified any residual spikes from the hourly NEE data using the method proposed by Papale et al. (2006) and modified by Barr et al. (2009). For each hour (i), the measure of change in NEE (d_i) from the previous ($i-1$) and next ($i+1$) time step is calculated as:

$$d_i = (\mathrm{NEE}_i - \mathrm{NEE}_{i-1}) - (\mathrm{NEE}_{i+1} - \mathrm{NEE}_i) \tag{6}$$

A spike is identified if the change is outside a given range:

$$\mathrm{Md} - \left(\frac{z \times \mathrm{median}|d_i - \mathrm{Md}|}{0.6745}\right) < d_i > \mathrm{Md} + \left(\frac{z \times \mathrm{median}|d_i - \mathrm{Md}|}{0.6745}\right) \tag{7}$$

where Md is the median of the differences (d_i), ±0.6745 are the quartiles for a standard normal distribution, and the constant z was conservatively set to 5 (Restrepo-Coupe et al., 2013).

2.2.2 Ecosystem respiration (R_{eco}) and gross ecosystem productivity (GEP)

Night-time hourly NEE values were corrected for periods of low turbulent mixing by removing them from the time series data. Low turbulent missing periods were determined when friction velocity (u^* in $\mathrm{m\,s^{-1}}$) was below a threshold value (u^*_{thresh}) as described in Restrepo-Coupe et al. (2013). Table 1 presents site-specific u^*_{thresh} values and the corresponding upper and lower confidence bounds.

Night-time NEE is assumed to be representative of ecosystem respiration (R_{eco}) and it is calculated by fitting R_{eco} to a second-order Fourier regression based on the day of the year (DOY) as in Richardson and Hollinger (2005):

$$R_{\mathrm{eco}} = f_o + s_1 \sin(\mathrm{Dpi}) + c_1 \cos(\mathrm{Dpi}) + s_2 \sin(2\mathrm{Dpi}) + c_2 \cos(2\mathrm{Dpi}) + e \qquad (8)$$

where, f_o, e, s_1, c_1, s_2, and c_2 are the fitted coefficients and $\mathrm{Dpi} = \mathrm{DOY} \times 360/365$ in radians. This method calculates R_{eco} with minimal use of environmental covariates. In order to determine the consistency of the Fourier regression method and the low friction velocity (u^*) filter on the modelled R_{eco} (directly dependent of night-time NEE values), we compared the results presented here to R_{eco} values based on the intercept of the relation (rectangular hyperbola) between NEE and $\mathrm{SW_{down}}$ (for no incoming radiation, $\mathrm{SW_{down}} = 0$; Suyker and Verma, 2001; Fig. S1 in the Supplement).

Gross ecosystem exchange (GEE) was calculated as the difference between NEE and R_{eco} ($\mathrm{GEE} = \mathrm{NEE} + R_{\mathrm{eco}}$). We defined gross ecosystem productivity (GEP) as negative GEE (positive values of GEP flux indicate carbon uptake). For a 16-day moving window, we fitted two rectangular hyperbolas on the relationship between incoming PAR and GEP observations (separating morning and afternoon values) as in Johnson and Goody (2011) and based on the Michaelis and Menten formulation (1913):

$$\mathrm{GEP} = \frac{\alpha \times \mathrm{GEP_{sat}} \times \mathrm{PAR}}{\mathrm{GEP_{sat}} + (\alpha \times \mathrm{PAR})} \tag{9}$$

where α is the ecosystem apparent quantum yield for CO_2 uptake (the initial slope), and $\mathrm{GEP_{sat}}$ is GEP at saturating light (the asymptote of the regression; Falge et al., 2001; Fig. 2). Our intention was to compare 16-day MODIS data to observations rather than to model a complete time series. We therefore, filled infrequent GEP missing values only if in a 16 day period there were 30 h of measurements.

We obtained similar seasonal patterns and good agreement using different methods for calculating GEP and R_eco (Fig. S1). We observed no statistically significant seasonal differences between calculating R_eco as the intercept of the light response curve (Falge et al., 2001) and NEE not subject to u^*_thresh correction ($R_\mathrm{eco\,LRC}$), to calculating R_eco using the Fourier regression method (slope ~ 0.87 and $R^2 = 0.94$ linear regression between $R_\mathrm{eco\,LRC}$ and R_eco). This comparison increased our confidence in using either method to derive GEP and R_eco fluxes from the EC data, the absolute values and the seasonality here presented.

Note that the term GEP includes gross primary productivity (GPP), which is defined as the amount of CO_2 fixed in photosynthesis plus the CO_2 from photorespiration (Waring and Running, 1998). Assuming negligible photorespiration, GEP and GPP have been used interchangeably when describing EC-derived photosynthesis (Restrepo-Coupe et al., 2013; Stoy et al., 2006). However, for this study we used the term GEP when derived from the tower-flux observations to differentiate it when compared to MODIS GPP (see next section).

2.2.3 Four measures of ecosystem photosynthetic potential: α, LUE, $\mathrm{GEP_{sat}}$, and Pc

Measures of photosynthetic potential constitute an attempt to separate the inherent vegetation properties that contribute to photosynthetic activity (GEP) from the effects of the meteorological influences on productivity. The variables α, LUE, $\mathrm{GEP_{sat}}$, and Pc were intended to represent an ecosystem property, a descriptor of the vegetation phenology similar to leaf area index (LAI) or above ground biomass (AGB). We calculated 16-day mean α and $\mathrm{GEP_{sat}}$, which are the two coefficients that define the GEP vs. PAR rectangular hyperbola (Eq. 5) as a measure of the vegetation structure and function (Fig. 2). Both α ($\mu\mathrm{mol\,CO_2\,mmol^{-1}}$) and $\mathrm{GEP_{sat}}$ ($\mu\mathrm{mol\,CO_2\,m^{-2}\,s^{-1}}$) values are known to vary with vegetation type, temperature, water availability and $\mathrm{CO_2}$ concentration. $\mathrm{GEP_{sat}}$ represents the ecosystem response at saturating levels of PAR, usually constrained by high vapour pressure deficit (VPD), air temperature (T_{air}), water availability, and foliar N, among other variables (Collatz et al., 1991; Ehleringer et al., 1997; Tezara et al., 1999). By contrast, α is measured at low light levels, when diffuse radiation is high (cloudy periods, sunset and sunrise). Ecosystem light use efficiency (LUE) was defined as the mean daily GEP/PAR ratio. Therefore, LUE includes the effect of day length, the radiation environment (diffuse vs. direct), water availability and other physical factors.

We used the relationships between tower measured GEP, PAR, and VPD to characterize the photosynthetic capacity of the ecosystem (Pc). Where Pc was defined as the average GEP for incoming radiation at light levels that are non-saturating – values between the annual daytime mean PAR $\pm 100\,\mu\mathrm{mol\,m^{-2}\,s^{-1}}$ (940, 1045, 788 and 843 $\mu\mathrm{mol\,m^{-2}\,s^{-1}}$ at HSP, ASP, TBR and CHO, respectively) and VPD ranges between annual daytime mean ±2 standard deviations (Fig. 2; Hutyra et al., 2007; Restrepo-Coupe et al., 2013). Pc was interpreted as a measure of the built capacity without taking into account the day-to-day changes in available light, photoperiod, and extreme VPD and PAR values. The derivation of Pc did not take into account other variables such as T_{air} or soil water content.

2.3 Remote sensing data

2.3.1 Moderate Resolution Imaging Spectroradiometer (MODIS)

We retrieved MODIS reflectances, VIs and other products from the USGS repository covering the four eddy flux locations. Data were subject to quality assurance (QA) filtering, and pixels sampled during cloudy conditions and pixels adjacent to cloudy pixels were rejected (for a complete list of QA rules see Table S1 in the Supplement). Other QA datasets and/or fields related to the above products that were not included on the original metadata were not examined as part of the quality filtering process.

At each site we extracted either a 1 km window (or a 1.25 km window depending on MODIS product resolution – see Table 2) centred on the location of the flux tower. The mean and standard deviation of all pixels were assumed to be representative of the ecosystem. The derivative data collection included the following MODIS data (also see Table 2):

MCD43A1: the 8-day 500 m (Collection 5) Nadir Bidirectional Reflectance Distribution Function (BRDF) Adjusted Reflectance (NBAR) product was used to derive the enhanced vegetation index ($\mathrm{EVI_{SZA30}}$) and the normalized vegetation index ($\mathrm{NDVI_{SZA30}}$) at fixed solar zenith angle of 30° (available for 2003 to 2013):

$$\mathrm{NDVI_{SZA30}} = \frac{\mathrm{NIR_{SZA30}} - R_{\mathrm{SZA30}}}{\mathrm{NIR_{SZA30}} + R_{\mathrm{SZA30}}} \tag{10}$$

$$\mathrm{EVI_{SZA30}} = \frac{G \times (\mathrm{NIR_{SZA30}} - R_{\mathrm{SZA30}})}{\mathrm{NIR_{SZA30}} + (\mathrm{C1} \times R_{\mathrm{SZA30}}) - (\mathrm{C2} \times -B_{\mathrm{SZA30}}) + L} \tag{11}$$

where R_{SZA30}, $\mathrm{NIR_{SZA30}}$ and B_{SZA30} are the red, near infrared, and blue band BRDF corrected reflectances, and coefficients $G = 2.5$, $\mathrm{C1} = 6$, $\mathrm{C2} = 7.5$, and $L = 1$ (Huete et al., 1994). Both VIs are measures of greenness and have been designed to monitor vegetation, in particular photosynthetic potential and phenology (Huete et al., 1994; Running et al., 1994). However, the EVI has been optimized to minimize the effects of soil background, and to reduce the impact of residual atmospheric effects.

We labelled the NBAR VIs as $\mathrm{EVI_{SZA30}}$ and $\mathrm{NDVI_{SZA30}}$ to differentiate them from the MOD13 VI product (EVI and NDVI), and emphasize the values here presented include a BRDF correction that is aimed to remove the influence of sun-sensor geometry on the reflectance signal (Schaaf et al., 2002).

MOD15A2: the Leaf Area Index ($\mathrm{LAI_{MOD}}$), and Fraction of Photosynthetically Active Radiation ($\mathrm{fPAR_{MOD}}$) absorbed by vegetation from atmospherically corrected surface reflectance products (Knyazikhin et al., 1999). Data were filtered to remove outliers present in the $\mathrm{fPAR_{MOD}}$ and $\mathrm{LAI_{MOD}}$ time series using Eq. (3). A threshold value of 6 for the z coefficient was calibrated to remove 8-day variations of ±50 % on $\mathrm{fPAR_{MOD}}$, and ±3–4 units in $\mathrm{LAI_{MOD}}$.

MOD17A2: the 8-day Gross Primary Production ($\mathrm{GPP_{MOD}}$) and Net Photosynthesis (PsnNet) (collection 5.1). The $\mathrm{GPP_{MOD}}$ is calculated using the formulation proposed by Running et al. (2000) and relies on satellite derived short-wave downward solar radiation ($\mathrm{SW_{down}}$), $\mathrm{fPAR_{MOD}}$, maximum light-use-efficiency ($\varepsilon_{\max}$) obtained from a biome-properties look-up table, and maximum daily VPD ($\mathrm{VPD_{max}}$) and minimum daily air temperature ($T_{\min}$) from forcing meteorology:

$$\mathrm{GPP_{MOD}} = \varepsilon\max \times 0.45 \times \mathrm{SW_{down}} \times \mathrm{fPAR_{MOD}} \times \mathrm{f}(\mathrm{VPD_{max}}) \times \mathrm{f}(T_{\min}) \tag{12}$$

where only the highest quality data were selected for the analysis.

MOD11A2: Daytime Land Surface Temperature ($\mathrm{LST_{day}}$) 8-day time-series was included in the analysis in order to study the effect of T_{air}, another important ecosystem carbon flux driver. Thus, as LST or skin temperature (temperature at the interface between the surface and the atmosphere) has been proven to be highly correlated to T_{air} (Shen and Leptoukh, 2011).

2.3.2 Satellite measures of precipitation (TRMM) and incoming solar radiation (CERES)

This study incorporated monthly 0.25° resolution precipitation data (1998–2013) in units of $\mathrm{mm\,month^{-1}}$ from the Tropical Rainfall Measuring Mission (TRMM) data product (3B43-v7) derived by combining TRMM satellite data, GOES-PI satellite data, and a global network of gauge data (Huffman et al., 2007). We used 1.0° resolution monthly surface shortwave flux down (all-sky) in $\mathrm{W\,m^{-2}}$ from the Clouds and the Earth's Radiant Energy System (CERES) experiment (Gesch et al., 1999). The CERES Energy Balanced And Filled top of the atmosphere (EBAF) Surface_Ed2.8 product provided fluxes at surface, consistent with top of the atmosphere fluxes (CERES- EBAF TOA; Kato et al., 2012). No quality control was performed on the rain ($\mathrm{Precip_{TRMM}}$) or short wave ($\mathrm{SW_{CERES}}$) satellite derived time series.

2.4 Mean values

All analyses were done on 16-day data, therefore, 8-day MODIS products were resampled to the match the selected temporal resolution. We interpolated lower frequency satellite remote sensing time series (e.g. CERES and TRMM), using a linear regression from the original dataset to 16-days, where the original value corresponds to the centre of the month defined as day 15, and the newly interpolated value will be representative of the middle of the 16-day period.

Mean fluxes and variables from the eddy covariance are reported on a 30 min or hourly basis. Daily averages were calculated if at least 45 out of 48, or 21 out of 24 data points were available for the day. Bi-weekly values were calculated if at least 4 out of the 16 days were available. For analysis and presentation purposes, we averaged all existing 16-day values of EC and RS data to produce a single year, seasonal cycle.

2.5 Evaluation of synchronicity between remote sensing and flux-tower data

We fitted Type II (orthogonal) linear regressions between GEP, Pc, α LUE, and $\mathrm{GEP_{sat}}$, and the different satellite products described above. We obtained an array of very simple models of productivity and photosynthetic potential. For example, $\mathrm{GEP_{RS}}$, where $\mathrm{GEP_{RS}} = b_0 + b_1 \times \mathrm{RS}$, b_0 and b_1 were site-specific coefficients, and RS are satellite derived products (EVI, fPAR, etc.). We compared the different models to the observations (GEP vs. GEP_{EVI}, GEP vs. GEP_{NDVI}, etc.) using Taylor single diagrams (Taylor, 2001), where the radial distances from the origin are the normalized standard deviation, and the azimuthal position is the correlation coefficient between the GEP_{RS} and GEP or any other measure of ecosystem photosynthetic potential (Fig. S2).

We determined at each site which combination of carbon flux and MODIS index showed good agreement based on statistical descriptors: coefficient of determination, *p* value, root-mean-square-error (RMSE), standard deviation (SD) of the observation and model, and the Akaike's Information Criterion (AIC). Thus, we analysed site-specific and cross-site multiple regression models to compare different biological (greenness) and environmental controls (precipitation, temperature, radiation) on productivity. In each ecosystem, GEP was modelled as a linear regression using a single independent variable, two-variables, and bivariate models that included an interaction term. For example: (1) $\mathrm{GEP} = b_0 + b_1 \times \mathrm{EVI}_{\mathrm{SZA30}}$, (2) $\mathrm{GEP} = b_0 + b_1 \times \mathrm{EVI}_{\mathrm{SZA30}} + b_2 \times \mathrm{SW}_{\mathrm{CERES}}$, and (3) $\mathrm{GEP} = b_0 + b_1 \times \mathrm{EVI}_{\mathrm{SZA30}} + b_2 \times \mathrm{SW}_{\mathrm{CERES}} + b_3 \times \mathrm{EVI}_{\mathrm{SZA30}} \times \mathrm{SW}_{\mathrm{CERES}}$, where b_0, b_1, b_2, and b_3 are fitted coefficients by a nonlinear mixed-effects estimation method. Additional models derived from the all-site regressions were compared to the site-specific results. We inferred ecosystem adaptation responses to climate (e.g. light harvest adaptation, water limitation, among other phenological responses) from the bivariate models. This analysis is useful for the interpretation of satellite derived phenology metrics and understanding the biophysical significance of different measures of greenness when incorporated into ESM as representative of vegetation status.

3 Results

3.1 Seasonality of in situ measurements

In this section we describe the seasonality of in situ meteorological measurements to better understand ecosystem carbon fluxes, and to contextualize the differences in vegetation responses to climate. In particular, we contrast seasonal patterns of air temperature (T_{air}), precipitation, and VPD across sites, and compare observations of the annual cycle of photosynthetic activity (productivity) and potential (biophysical drivers of productivity) for each ecosystem.

With the exception of HSP, all sites showed strong seasonality in T_{air} (Fig. 3). However, the timing of mean daily T_{air} minimum and maximum, and the amplitude of the annual values, varied according to site. The smallest range in T_{air} (5 °C) occurred at the northern tropical savanna (HSP), and the largest amplitude (15 °C) occurred at the southern temperate locations (CHO and TBR). The annual cycle of VPD followed T_{air} at all locations except HSP where summer and autumn rains (February–March) lead to a decrease in VPD (Fig. 3). Precipitation at HSP was higher and more seasonal than at any other site with a mean monthly rainfall of 152 mm (1824 mm yr^{-1}) and ranging from 1 to 396 mm month^{-1}. Incoming radiation at the tropical savanna site (HSP) did not show clear seasonality (Fig. 3). In this tropical savanna (latitude 12.49° S) the summer solstice, where top of the atmosphere (TOA) radiation is highest, coincides with monsoonal cloudiness resulting in reduced surface radiation. By contrast, at temperate sites like CHO and TBR, the difference in mean daily PAR between summer and winter was $\sim$ 460 µmol m^{-2} s^{-1}. Rainfall was aseasonal at TBR ($\sim$ 78 mm month^{-1}) and was very low at the semi-arid sites of CHO and ASP with mean precipitation values of 34 and 37 mm month^{-1} respectively.

Productivity in the four ecosystems ranged from a high at HSP and TBR (Fig. 4; peak 16-day multi-year average GEP of 8.4 and 7.7 g C m^{-2} d^{-1} respectively) to a low at CHO and ASP (peak 16-day annual average GEP average of 2.4 and 3.4 g C m^{-2} d^{-1} respectively; Fig. 4). There was a clear seasonal cycle in photosynthetic activity with maxima in the summer at HSP and TBR (November–March) and in the autumn (March–April) at ASP and CHO. The peaks were broader at TBR than at HSP and at ASP (Fig. 4). An additional short-lived increase in GEP was apparent at ASP in the spring (October) before the summer wet period (Fig. 4a). Figures S3 and S4 show the diel cycles of VPD, GEP and other meteorological and flux variables in example summer (January) and winter months (July).

Vegetation phenology, as indicated by the seasonal cycle of photosynthetic potential (Pc, LUE, α, and $\mathrm{GEP_{sat}}$), diverged from photosynthetic activity (GEP) at the southern locations of TBR and CHO as shown by the differences in the timing of maximum and minimum GEP compared to vegetation phenology (Figs. 4 and S5). At the tropical savanna site (HSP), ecosystem quantum yield (α) increased gradually in the spring (September), reaching a maximum during the summer month of January in synchrony with GEP. In the sclerophyll forest (TBR), α remained at a constant value of $\sim 1.4\,\mathrm{g\,C\,MJ^{-1}}$ until the middle of the autumn (April–May) when it reached a value of $1.76\,\mathrm{g\,C\,MJ^{-1}}$. Maximum $\mathrm{GEP_{sat}}$ occurred during the summer at this site ($\sim 36\,\mathrm{g\,C\,m^{-2}\,d^{-1}}$) and gradually decreased by the start of the autumn with a winter minimum ($20\,\mathrm{g\,C\,m^{-2}\,d^{-1}}$). At TBR, the $\mathrm{GEP_{sat}}$ and α were out-of-phase (Fig. 4) and although seasonality was limited in $\mathrm{GEP_{sat}}$ and α, neither of them matched seasonal fluctuations in VPD (cf. Figs. 3 and 4). Similar to $\mathrm{GEP_{sat}}$, LUE decreased during the summer months and experiences a winter maximum opposite to the annual cycle of GEP. Given the high degree of seasonality of GEP at TBR, it is interesting that the photosynthetic potential was comparatively less seasonal and asynchronous to productivity. Figure S5 shows the relationships between the different measures of ecosystem performance indicating that they are not always linear.

3.2 Seasonality of satellite products

In the tropical savanna (HSP) the annual cycles of RS products synchronously reached an early summer maximum in January, and high values extended throughout the autumn (Fig. 4d and e). By contrast at CHO, both $\mathrm{NDVI_{SZA30}}$ and $\mathrm{EVI_{SZA30}}$ peaked in autumn–winter, coinciding with the lowest GEP values (Fig. 4p and s). $\mathrm{EVI_{SZA30}}$ and $\mathrm{NDVI_{SZA30}}$ at ASP captured the autumn peak in GEP with a maximum in March, however, a spring VI minimum (November) was not observable in GEP. At the two semi-arid sites (ASP and CHO), $\mathrm{fPAR_{MOD}}$ was relatively aseasonal, and the amplitude of the annual cycle was ~ 0.09, with a 0.25–0.34 range at CHO and lower values between 0.17–0.26 at ASP (Fig. 4o). $\mathrm{LAI_{MOD}}$ at CHO reached a maximum of 0.50 during the autumn (March) and a spring minimum (September) of 0.39. At ASP, the LAI_{MOD} product ranged from 0.17 (December) to 0.27 (April; Fig. 4t). Most RS products (e.g. EVI_{SZA30} and LAI_{MOD}) showed no clear seasonality at TBR (Fig. 5i and j).

$fPAR_{MOD}$ vs. $NDVI_{SZA30}$ were highly correlated at all sites ($R^2 > 0.7$, $p < 0.01$) with the exception of the sclerophyll forest (TBR) where $NDVI_{SZA30}$ remained constant in the 0.68–0.83 range ($R^2 = 0.01$; Fig. S6). At the sclerophyll forest site (TBR), the $NDVI_{SZA30}$ reached values close to saturation. Similar to $fPAR_{MOD}$ vs. $NDVI_{SZA30}$, EVI_{SZA30} vs. $NDVI_{SZA30}$ was highly correlated ($R^2 = 0.96$, all-site regression). However, the timing of minimum and maximum between $NDVI_{SZA30}$ and EVI_{SZA30} differed at CHO and HSP (Figs. 4 and 5d and s).

3.3 Relationship between MODIS EVI and GPP and in situ measures of ecosystem photosynthetic activity (GEP)

In this study we used a simple linear model to predict GEP from EVI_{SZA30} and GPP_{MOD}. We observed three patterns. First, in the tropical savanna site (HSP) there was a highly significant correlation between photosynthetic activity and EVI_{SZA30}, where EVI_{SZA30} explained 82 % of GEP (Fig. 5a). Similarly at ASP, productivity was statistically related to EVI_{SZA30} ($R^2 = 0.86$, $p < 0.01$). However, GPP_{MOD} only explained 49 % of GEP at HSP and 48 % at ASP (Fig. 5e and g).

A second pattern was observed in the sclerophyll forest site (TBR), where the relationship between GEP and EVI_{SZA30} was not statistically significant ($R^2 < 0.01$ and $p = 0.93$, Fig. 5b). At TBR there was a clear seasonal cycle in GEP (low in winter and high during the summer) that was not captured by the small amplitude of the satellite derived data (Fig. 3). Of the four ecosystems examined, TBR was the only site where GPP_{MOD} showed an improvement (higher predictive value of GEP) compared to EVI_{SZA30}. However, as reported in previous works (Leuning et al., 2005), the GPP_{MOD} product was unable to capture the seasonality of the sclerophyll forest as it underestimated the observed summer peak in GEP which corresponded to a second minimum in GPP_{MOD}.

Finally, at the semi-arid site (CHO), we observed R^2 values significantly different from 0 but small R^2 0.34 and 0.24 ($p < 0.01$) for GEP vs. EVI_{SZA30} and GEP vs. GPP_{MOD}, respectively. This, demonstrated the low predictive power of both satellite products to determine seasonal GEP values at this particular Mediterranean ecosystems. In particular the GEP_{EVI} and GPP_{MOD} models tended to underestimate productivity at low levels (Fig. 5d and h).

The relationship between productivity and EVI_{SZA30} was complex across the different Australian ecosystems (Fig. 5). The semi-arid site of CHO and the sclerophyll forest of TBR are particularly interesting because of the inability of EVI_{SZA30} to seasonally replicate GEP (Fig. 5). An additional analysis that considers the amplitude and phase of the annual cycle (based on all available 16-day observations) was conducted using Taylor plots (Fig. S7). This analysis showed that EVI_{SZA30} was in-phase and able to predict the range of productivity values at HSP and ASP, while at the CHO site the EVI_{SZA30} captured the amplitude of seasonal GEP, however, the linear model was out-of-phase. At TBR, the EVI_{SZA30}-based model consistently preceded in situ observations (asynchronous) and exaggerated GEP seasonality (ratio between the standard deviation of the model and observations was 4.98).

3.4 Relationship between EVI_{SZA30} and measures of photosynthetic potential (α, LUE, GEP_{sat}, and Pc)

In this section we reconsider our understanding of EVI_{SZA30} by relating it to different measures of photosynthetic potential (α, LUE, GEP_{sat}, and Pc) across the four sites (Fig. 6). Similar to Sect. 3.3, we used a very simple linear model in which EVI_{SZA30} was expected to predict α, LUE, GEP_{sat}, and Pc. In the regression models for photosynthetic potential the R^2 values were similar to the GEP models for HSP and ASP (cf. Fig. 6c and g). However, EVI_{SZA30} vs. α at HSP R^2 was relatively low ($R^2 < 0.4$,

$p < 0.01$). At the CHO site, the $\mathrm{EVI}_{\mathrm{SZA30}}$-based model was able to improve the timing and amplitude of the annual cycle when used to calculate LUE, Pc and $\mathrm{GEP}_{\mathrm{sat}}$ instead of GEP (Figs. 6 and S7).

At the sclerophyll forest site (TBR) the $\mathrm{EVI}_{\mathrm{SZA30}}$ was able to predict vegetation phenology rather than productivity. For example, we observed that Pc (but not α) was strongly related to $\mathrm{EVI}_{\mathrm{SZA30}}$ ($R^2 = 0.16$, $p < 0.01$; Fig. 6 and Table S4). Even though, the regressions between LUE, $\mathrm{GEP}_{\mathrm{sat}}$, and Pc against $\mathrm{EVI}_{\mathrm{SZA30}}$ showed higher correlation ($R^2 \sim 0.13$, $p < 0.01$) than the GEP vs. $\mathrm{EVI}_{\mathrm{SZA30}}$ relationship ($R^2 = 0.04$, $p = 0.25$) at TBR, R^2 values were still low. However, the low R^2 can be explained by the small dynamic range of both seasonal measures of photosynthetic potential and $\mathrm{EVI}_{\mathrm{SZA30}}$ (cf. Figs. 4 and 6).

3.5 Satellite products compared to flux tower based measures of ecosystem potential

In this section we explore other MODIS products ($\mathrm{LAI}_{\mathrm{MOD}}$, $\mathrm{fPAR}_{\mathrm{MOD}}$, and $\mathrm{NDVI}_{\mathrm{SZA30}}$) to determine if the predictive power of $\mathrm{EVI}_{\mathrm{SZA30}}$ as a measure of photosynthetic potential (e.g. Pc) can be generalised across other satellite-derived biophysical parameters. We aimed to determine for each location, which of the MODIS products capture the seasonality and phenology of vegetation, thereby gaining some insight into the significance of the different VIs and other satellite derived ecosystem drivers. At HSP and ASP the MODIS $\mathrm{LAI}_{\mathrm{MOD}}$, $\mathrm{fPAR}_{\mathrm{MOD}}$ and VIs showed a larger or similar correlations to LUE and Pc in comparison to GEP (Table S4, Fig. 7a, b, i and j, respectively). At HSP, ASP, and CHO, based on our analysis using Taylor plots, most RS products were in-phase with the various measures phenology ($R^2 > 0.8$ and low RMSE; Figs. 7 and S2 and Table 4). However, there was a tendency for most RS indices to underestimate the seasonality of the LUE annual cycle at all sites (i.e., standard deviation was smaller for $\mathrm{LUE}_{\mathrm{RS}}$ than the observed, Fig. 7). With exception to TBR, all products were able to capture seasonal changes in Pc (Figs. 6 and 7).

Similar to $\text{EVI}_{\text{SZA30}}$, most of the MODIS indices, and in particular fPAR_{MOD} and LAI_{MOD}, showed strong linear relationships with LUE and Pc at the Mediterranean ecosystem CHO, where the introduction of phenology represented an important improvement over the RS-derived models (Figs. 6 and 7). Similarly, comparable to $\text{EVI}_{\text{SZA30}}$, other MODIS products were unable to replicate GEP at TBR (Fig. 7). However, the small amplitude of seasonality in LUE and Pc were well characterized by LUE_{RS} and Pc_{RS}, including a winter maximum similar to that in LUE (Fig. 4), despite underestimating the annual seasonal cycle in the sclerophyll forest (Figs. 4 and 7e–h).

3.6 Multi-biome derived linear relationships between VIs and photosynthetic potential (phenology) and activity (productivity)

Our objective was to investigate if one relation fits all flux sites, and which RS products and equations would enable us to extend our analysis from these four key Australian ecosystems to a continental scale. The all-site relationship for MODIS $\text{EVI}_{\text{SZA30}}$, $\text{NDVI}_{\text{SZA30}}$, LAI_{MOD}, and fPAR_{MOD} products (in that order) show the best agreement (phase and amplitude) to seasonality of LUE and Pc (Fig. 7). Correlations increased for relationships built using data for all the ecosystems instead of the site-specific equations with the exception of the ASP site (Figs. 7 and 8 and Table 3).

Improvements in how satellite products can model biological drivers (photosynthetic potential) instead of productivity per se, are clearly seen at the evergreen temperate forest of TBR. At TBR the relationship between GEP and any of the satellite products was not statistically significant ($R^2 < 0.1$) with the exception of LST_{day} (Figs. 5 and 7). However, skin temperature (LST_{day}) is a meteorological driver or constraint rather than a direct measure of productivity, and the low all-site LST_{day} vs. GEP correlation was an indication of this ($R^2 = 0.66$, $p = 0.03$; Fig. 8).

The wet sclerophyll forest introduced the greatest uncertainties to the linear models across all sites (Fig. 8). For example, regressions involving $\text{EVI}_{\text{SZA30}}$ were exponential, therefore, significantly increasing GEP and LUE translated into slightly higher $\text{EVI}_{\text{SZA30}}$

values, a behaviour mostly driven by the observations at TBR. In particular, the relationship between LUE vs. fPAR_{MOD} and LUE vs. $\text{NDVI}_{\text{SZA30}}$ at TBR were problematic as fPAR_{MOD} and $\text{NDVI}_{\text{SZA30}}$, appeared to "saturate" at 0.9 and 0.8, respectively (Fig. 8).

$\text{EVI}_{\text{SZA30}}$ explained 81 % of Pc seasonality based on an all-site regression (Table S4). Similarly, $\text{NDVI}_{\text{SZA30}}$ showed a high coefficient of determination (0.70 for GEP_{NDVI}, 0.75 for LUE_{NDVI}, and 0.79 for Pc_{NDVI}; Table S4). The null hypothesis of no correlation was rejected ($p < 0.01$) for all regressions between MODIS VIs, LAI_{MOD} and fPAR_{MOD} vs. photosynthetic potential (phenology) and activity (productivity; Table S4). However, statistical significance of GEP vs. $\text{GEP}_{\text{RS,}}$ was driven by the ASP and HSP ecosystems.

Multiple linear regression models used to predict GEP by combining satellite derived meteorology and biologic parameters (Table 3) showed large correlations when both drivers were introduced (meteorology and vegetation phenology), with the exception of the TBR site where SW_{CERES} and LST_{day} explained 60 and 58 % of GEP, respectively, and the ASP and HSP sites where $\text{EVI}_{\text{SZA30}}$ and $\text{NDVI}_{\text{SZA30}}$ explained ~ 84 and ~ 80 % of the variations in GEP, respectively. In particular, at the HSP site, no significant improvement to the GEP model was obtained when combining MODIS VIs with any meteorological variable (R^2 remain similarly high $R^2 \sim 0.82$). By contrast, at the ASP site, $\text{EVI}_{\text{SZA30}}$, satellite derived incoming short wave (SW_{CERES}), and the interaction of both significantly increased model correlation with an R^2 of 0.88 and a lower AIC (Akaike's Information Criterion as a measure of model quality) when compared to models relying only on $\text{EVI}_{\text{SZA30}}$ ($R^2 = 0.85$, AIC = 64) or SW_{CERES} ($R^2 = 0.02$, AIC = 209) (Table 3). Similar results were obtained for those regressions driven by $\text{EVI}_{\text{SZA30}}$ and precipitation at this rainfall pulse driven site ($R^2 = 0.88$, AIC = 42). At the CHO site, temperature-greenness models were highly correlated to GEP ($R^2 > 0.64$), however, the best results (higher R^2 and lower AIC) were obtained for radiation–greenness models, explaining 71 % ($\text{EVI}_{\text{SZA30}} - \text{SW}_{\text{CERES}}$ and $\text{NDVI}_{\text{SZA30}} - \text{SW}_{\text{CERES}}$) of GEP. For a complete version of Table 3 that includes all available variable combinations, see Table S3.

4 Discussion

4.1 Derivation of measures of photosynthetic potential at tropical savannas, sclerophyll forests and semi-arid ecosystems

In this study we were able to separate the biological (vegetation phenological signal) from the climatic drivers of productivity using eddy-covariance carbon exchange data. Different measures of vegetation photosynthetic potential (α, LUE, $\mathrm{GEP_{sat}}$ and Pc) have different biophysical meanings, therefore, we were able to establish physiological explanations for describing why and which RS products and environmental variables relate to them at each ecosystem. For example, $\mathrm{GEP_{sat}}$ measured at high levels of PAR is prone to be influenced by various environmental factors (VPD, T_{air} and soil water availability) and therefore may be a good indicator of canopy stress. As observed at HSP, $\mathrm{GEP_{sat}}$ was highly and negatively correlated to periods of low precipitation and negatively correlated with VPD (Table S4). Seasonal values of $\mathrm{GEP_{sat}}$ at the semi-arid sites (CHO and ASP) did not show a direct relationship with VPD or precipitation. This does not mean that there is no effect of atmospheric demand or soil moisture content on carbon fluxes at shorter time scales (hourly or daily). Compared to $\mathrm{GEP_{sat}}$, we expected α to be less dependent of VPD and better reflect vegetation phenology, as α represents the canopy photosynthetic response at low levels of PAR characteristic of cloud cover (diffuse light) during early morning or late afternoon periods (Kanniah et al., 2012, 2013). However, among all measures of phenology, α showed one of the lowest site-specific correlations when compared to any of the RS products presented on this study. Our results show that LUE and Pc showed the best correlations to VIs. Confirmation that this research deals less with the instantaneous responses ($\mathrm{GEP_{sat}}$ and α) and rather focuses on the mid-term, 16-day seasonal descriptors of vegetation phenology (Pc and LUE).

The influence of other environmental factors apart from PAR and VPD, such as soil water content and T_{air}, is difficult to isolate from the derivation of vegetation descriptors (e.g. specific leaf area, plant chlorophyll and water content) and is probably inherent to ecosystem responses and adaptation to climate, resource competition, and herbivory, among other factors. Moreover, to what degree it is feasible to untangle the relations between climate and vegetation is complex and not well understood, as the feedback processes are essential in ecosystem function (leaf flush, wood allocation, among other vegetation strategies respond to available resources). Our results show that VIs were highly related to Pc, which is interpreted as a phenology descriptor that does not consider the day-to-day changes in available light or photoperiod or the vegetation response to high and low VPD and PAR values. By contrast, implicit in the derivation of LUE were the day length and anomalous climatic conditions. This finding has important implications when using EC data for the validation of satellite derived phenology.

4.2 Seasonality and comparisons between satellite products and flux tower based measurements of carbon flux: photosynthetic activity (productivity) and potential (phenology)

Previous satellite derived models of productivity usually apply to locations where the seasonality of GEP is synchronous with climatic and vegetation phenology drivers (Mahadevan et al., 2008; Sims et al., 2008; Wu et al., 2010; Xiao et al., 2004), such as in temperate deciduous forests, where temperature and incoming radiation coincide with changes in ecosystem structure and function (e.g. autumn sub-zero temperatures may initiate leaf abscission; Vitasse et al., 2014). In our analysis, productivity was synchronous with all measures of photosynthetic potential only at the savanna site (HSP), where clouds and heavy rainfall in the summer wet season resulted in low VPD, reduced TOA (aseasonal PAR), and minimal fluctuations in T_{air}. At HSP, we observed a consistently large correlation between MODIS VIs and productivity and no improvement in GEP when accounting for meteorology. Moreover, the highly significant $\mathrm{EVI}_{\mathrm{SZA30}}$ vs. GEP relationship at HSP could be generalised to other satellite derived biophysical products.

Arid and semi-arid vegetation dominate ~ 75 % of the Australian continent, and at these ecosystems a characteristic mix of grasses (understory) and woody plants (overstory) contribute to total annual GEP at different times of the year. More importantly, the phenology of grasses and trees are driven by, or respond differently to, various climatic drivers (e.g. trees greening up after spring rainfalls while grasses remain dormant; Cleverly et al., 2015). The changing seasonal contributions to the reflectance signal and to GEP are generally related to soil water content thresholds. Our study presents two semi-arid *Acacia* and *Eucalyptus* woodlands where we found that models relating VIs with photosynthetic potential (phenology), rather than activity (productivity), improved the predictive power of RS greenness indices (CHO) or showed similar statistical descriptors (ASP). At the woodland *Acacia* site, $\mathrm{LAI}_{\mathrm{MOD}}$ and $\mathrm{fPAR}_{\mathrm{MOD}}$ overestimated the periods of low capacity (associated with browndown phases; Ma et al., 2013). This can be better understood if we account for small but non-negligible photosynthetic activity in *Acacia* after the summer rains have ended (Cleverly et al., 2013; Eamus et al., 2013). At this particular site (ASP), the high $\mathrm{LAI}_{\mathrm{MOD}}$ and VIs observed during dormancy may not be interpreted as high photosynthetic potential. Satellite data, and even some ground-based measurements of $\mathrm{LAI}_{\mathrm{MOD}}$, cannot differentiate between the different fractional components: photosynthetic active vegetation (fPAV), and non-photosynthetic vegetation (fNPV). Future work requires phenocams or biomass studies in which fPV and fNPV may be spectrally or mechanically separated.

In low productivity ecosystems (ASP and CHO), satellite and EC data/noise ratio may have a considerable effect on the site-specific regressions (e.g. sun geometry influence on VIs seasonal values, and EC uncertainties). However, differences between ASP and CHO regressions (e.g. $\mathrm{EVI}_{\mathrm{SZA30}}$ is highly correlated to GEP only at ASP) and the fact that the VI product has been corrected for BRDF effects, increases our confidence on the analysis presented here. Moreover, the lower VIs vs. GEP correlation values obtained at CHO compared to ASP could be attributed to Mallee site productivity being more dependent on meteorological drivers than photosynthetic potential, or GEP being driven by climate (e.g. autumn precipitation – when Pc remains constant) or vegetation phenology (e.g. summer LAI and canopy chlorophyll content, among others) at different times of the year.

Similar to Mediterranean ecosystems (CHO), in sclerophyll forests (TBR), the VIs were unable to replicate seasonality in GEP. In particular, the dominant species of sclerophyll forests, *Eucalyptus*, *Acacias* and *Banksias*, show very little seasonal variation in canopy structure as seen in aseasonal LAI observations (Zolfaghar, 2013), and leaf longevity (Eamus et al., 2006). Leaf quantity (e.g. LAI) and quality (e.g. leaf level photosynthetic assimilation capacity) are two key parameters in driving photosynthetic potential; when these are aseasonal, asynchronous or lagged, they may confound the interpretation of seasonal measures of greening. Thus, the observed increasing predictive power of VIs as a measure of photosynthetic potential (e.g. $\text{EVI}_{\text{SAZ30}}$ vs. Pc, $R^2 = 0.16$ at TBR) may not be comparable to similar relationships at sites where vegetation phenology showed a larger dynamic range (e.g. $\text{EVI}_{\text{SZA30}}$ vs. Pc, $R^2 = 0.79$ at HSP).

4.3 Considerations for the selection of RS data to be used on GEP models and phenology validation studies

This study reports high correlations for Pc vs. $\text{EVI}_{\text{SZA30}}$ ($R^2 = 0.81$) and Pc vs. $\text{NDVI}_{\text{SZA30}}$ ($R^2 = 0.80$). The fact that a brighter soil background results in lower NDVI values than with a dark soil background for the same quantity of partial vegetation cover (Huete, 1988; Huete and Tucker, 1991) may have a positive effect in the all-site Pc vs. $\text{NDVI}_{\text{SZA30}}$ regressions (increase R^2). At certain times the ASP and CHO sites were at the low end of the vegetation activity range, and photosynthetic potential of the understory is thus highly related to soil water content. Darkened soils following precipitation generally result in higher NDVI values for incomplete canopies (Gao et al., 2000) and may suggest higher vegetation or soil biological crust activity. However, caution is needed when using fPAR_{MOD} and other products as we observed a threshold value above which in situ changes were undetectable (e.g. MODIS fPAR > 0.9,

$NDVI_{SZA30} > 0.8$). This might have been due to the NDVI saturating at high biomass (Huete et al., 2002; Santin-Janin et al., 2009).

Temperature-greenness models of GEP (Sims et al., 2008; Xiao et al., 2004) take into account the meteorological and biophysical drivers that determine productivity. Nevertheless, correlations between photosynthetic characteristics and LST_{day} were weaker than for VIs. Moreover, if the seasonality of GEP is driven by local climatology, as in the case of TBR where GEP was statistically correlated to LST_{day}, our intent is to understand the relation between vegetation characteristics and RS products rather than indiscriminately use any satellite-derived index to describe phenology or photosynthetic potential. Our study demonstrates that multiple linear regression models that combine satellite derived meteorology and biological parameters to describe GEP fit better when both drivers are introduced rather than when only one factor drives the relation (a single meteorology or greenness variable). However, two exceptions to this rule were observed: (1) at TBR where SW_{CERES} was able to explain 60 % of GEP, and (2) in the tropical savanna at HSP where EVI_{SZA30} was able to explain ~ 82 % of the variation in GEP, and where we did not obtain any significant improvement to the GEP model when combining MODIS VIs and any meteorological variable (R^2 remain similarly high $R^2 > 0.82$). In summary, at evergreen sclerophyll forests, even when GEP is highly seasonal, GEP is driven by meteorology as seen by the fact that most of the measures of photosynthetic potential showed small seasonal changes, similar to different MODIS products. By contrast, sites where most of the GEP seasonality was driven by vegetation status (Pc as a proxy) rather than the meteorological inputs (PAR, air temperature and precipitation), or where meteorology and phenology were synchronous, VIs were strongly correlated to both GEP and Pc (e.g. tropical savanna). This was in agreement with the expectation than RS products constitute a measurement of ecosystem photosynthetic potential rather than productivity per se.

In summary, our analysis shows how MODIS greenness indices were able to estimate different measures of ecosystem photosynthetic potential across biomes. At only one site (TBR) was there very little seasonal variation in EVI_{SZA30}, compared to other evergreen ecosystems. Both the strong correlations among VIs and Pc from in situ eddy covariance carbon flux measurements at the remaining sites and the positioning of each ecosystem along a continuum of MODIS-derived variables representing vegetation phenology confirms the usefulness of satellite products as representative of vegetation structure and function. This research confirms the viability of satellite-derived phenology to be validated and more importantly, understood, using eddy-flux measurements of Pc. However, an increase in effort in determining seasonal patterns of carbon allocation (partition between leaves and wood), understory and overstory responses, and leaf carbon assimilation and chlorophyll content over time, may be required to obtain a more meaningful understanding of RS indices and their biophysical significance. Moreover, the reader should be aware that rapid changes in vegetation phenology (e.g.α and GEP_{sat}) caused by short-term environmental stresses (e.g., temperature, humidity, soil water deficit or waterlogging) may not be accurately estimated by RS products and require the employment of in situ high frequency optical measurements (e.g. phenocams), or land surface vegetation models, or direct eddy covariance measurements.

For this study we included all available 16-day data corresponding individually to more than 10 years at HSP and TBR, and two to three years at CHO and ASP. The long-term sampling implies that we were likely to be capturing a large range in mean ecosystem behaviour. RS products may over- or under-represent the canopy response to periods of extreme temperature and precipitation, although the time series in this study included warmer than normal years and heat waves, e.g. 2012–2013 (BOM, 2012, 2013; Van Gorsel, 2015) and wetter than normal years e.g. 2011(Fasullo et al., 2013; Poulter et al., 2014) that lead to larger than normal GEP at ASP and CHO (Cleverly et al., 2013; Eamus et al., 2013; Koerber et al., 2015). It is beyond the scope of this work to evaluate the inter-annual variability of the vegetation responses to disturbance (e.g. insect infestation or fire) or extreme climatic events (e.g. flooding or long term drought). Improvements to satellite derived phenology can be related to an increasing number of EC sites and samples thereby emphasizing the importance of long-term time measurements and sampling of diverse ecosystems.

5 Conclusions

Tower derived data of fluxes offer much more than simply validating and/or calibrating remote sensing products and models. An understanding of why satellite vs. flux tower relationships hold, or do not hold, greatly contribute to our comprehension of carbon cycle mechanisms and scaling factors at play. This is a significant improvement from using an empirical regression and "best performing" mentality. We have shown how $\mathrm{EVI_{SZA30}}$ was unable to represent GEP in the sclerophyll forest of Tumbarumba (TBR) and at the Mediterranean ecosystem of Calperum–Chowilla (CHO). This result extends across satellite products overall: MODIS $\mathrm{GPP_{MOD}}$, $\mathrm{LAI_{MOD}}$, $\mathrm{fPAR_{MOD}}$, and other VIs. The relationship between RS products and GEP was only clear when productivity was driven by either: (1) ecosystem phenology and climate, synchronously driving GEP, as was observed at ASP, and similar to many temperate deciduous locations, or (2) solely by the vegetation photosynthetic potential, as observed at the tropical savanna site of Howard Springs (HSP). For example, at HSP, radiation and temperature were constant across the year, although ecosystem photosynthetic activity (GEP) and potential (e.g. Pc and LUE) was highly seasonal. However, RS products do not follow GEP when either: (3) phenology is asynchronous to key meteorological drivers and GEP is driven by one or the other at different times of the year along the spectrum between meteorological driven and phenology driven ecosystems, as we observed at the Mediterranean woodland of Calperum–Chowilla (CHO); or when (4) productivity is driven by meteorology (PAR, T_{air}, soil water availability, VPD, or different combinations) and the vegetation photosynthetic potential is aseasonal, as observed in the sclerophyll forest of Tumbarumba (TBR). At TBR, changes in productivity were driven by incoming solar radiation ($\mathrm{SW_{down}}$) and vegetation photosynthetic potential remained relatively constant during the whole year, represented by the small amplitude of the annual cycles in Pc, LUE, and other measures of phenology (true evergreen forest).

This research contributes to our understanding of the meaning and shortcomings of satellite VIs in determining vegetation photosynthetic potential at different and complex Australian ecosystems, in particular at semi-arid ecosystems with high VPDs in summer and winter rainfall regimes and sclerophyll forests characterized by invariant canopy structure and long-life leaf span. The all site linear regressions can be used to extrapolate in situ measures of phenology to continental-wide and longer time scales. In general, the effect of deriving all-sites regressions between the satellite products and photosynthesis (independently of biome type) is to obtain more robust linear models. In particular, vegetation indices ($\mathrm{NDVI_{SZA30}}$ and $\mathrm{EVI_{SZA30}}$) were able to replicate the amplitude and timing of the ecosystem light use efficiency (LUE) and photosynthetic capacity (Pc). This has important implications when validating satellite derived phenology products (e.g. start, peak and end of the growing season) against eddy covariance flux observations. However, based on the all-site relations we report the saturation of $\mathrm{fPAR_{MOD}}$ and $\mathrm{NDVI_{SZA30}}$, and this restricts the usefulness of these products in comparatively low biomass ecosystems (savannas and arid and semi-arid savannas and woodlands).

The Supplement related to this article is available online at doi:10.5194/bgd-12-19213-2015-supplement.

Acknowledgements. This work was supported by an Australian Research Council Discovery Research Grant (ARC DP110105479) “Integrating remote sensing, landscape flux measurements, and phenology to understand the impacts of climate change on Australian landscapes and the Australian Government’s Terrestrial Ecosystems Research Network”. TERN (www.tern.org.au/) is a research infrastructure facility established under the National Collaborative Research Infrastructure Strategy and Education Infrastructure Fund (Super Science Initiative) through the Department of Industry, Innovation, Science, Research and Tertiary Education.

We utilized data collected by grants funded by the Australian Research Council (DP0344744, DP0772981 and DP130101566). J. Beringer is funded under an Australian Research Council Future Fellowship (ARC FT110100602).

The authors would like to thank our collaborators Professor Scott R. Saleska, Sabina Belli, and Piyachat Ratana. Special acknowledgement to Tim Lubcke, Rolf Faux, and Nicole Grant for technical support at different OzFlux sites.

We show our respect and acknowledge the people, the traditional custodians of the Land, of Elders past and present of the Arrernte Nation at Alice Springs, the Wiradjuri people at Tumbarumba, the Meru people at Calperum–Chowilla and the Woolna nation at Howard Springs.

References

Baldocchi, D.: Measuring fluxes of trace gases and energy between ecosystems and the atmosphere – the state and future of the eddy covariance method, Glob. Change Biol., 20, 3600–3609, doi:10.1111/gcb.12649, 2014.

Baldocchi, D., Falge, E., Gu, L., Olson, R., Hollinger, D., Running, S., Anthoni, P., Bernhofer, C., Davis, K., Evans, R., Fuentes, J., Goldstein, A., Katul, G., Law, B., Lee, X., Malhi, Y., Meyers, T., Munger, W., Oechel, W., Paw, K. T., Pilegaard, K., Schmid, H. P., Valentini, R., Verma, S., Vesala, T., Wilson, K., and Wofsy, S.: FLUXNET: a new tool to study the temporal and spatial variability of ecosystem–scale carbon dioxide, water vapor, and energy flux densities, B. Am. Meteorol. Soc., 82, 2415–2434, doi:10.1175/1520-0477(2001)082<2415:FANTTS>2.3.CO;2, 2001.

Baldocchi, D. D.: Assessing the eddy covariance technique for evaluating carbon dioxide exchange rates of ecosystems: past, present and future, Glob. Change Biol., 9, 479–492, doi:10.1046/j.1365-2486.2003.00629.x, 2003.

Barr, A., Hollinger, D. Y., and Richardson, A. D.: CO_2 Flux Measurement Uncertainty Estimates for NACP, AGU Fall Meeting, December 2009, abstract number B54A-04B, 2009.

Beringer, J., Hutley, L. B., Tapper, N. J., and Cernusak, L. A.: Savanna fires and their impact on net ecosystem productivity in north Australia, Glob. Change Biol., 13, 990–1004, doi:10.1111/j.1365-2486.2007.01334.x, 2007.

Beringer, J., Cleverly, J., Eamus, D., Van Gorsel, E., Hutley, L. B., Meyer, W. S., and Macfarlane, C.: An introduction to the Australian flux tower network – OzFlux, Biogeosciences, in this issue, 2015.

BOM: Special Climate Statement 41 – Extreme November heat in Eastern Australia, Australian Bureau of Meteorology, Melbourne, Australia, 2012.

BOM: Special Climate Statement 45 – a Prolonged Autumn Heatwave for Southeast Australia, Australian Bureau of Meteorology, Melbourne, Australia, 2013.

CERES – Clouds and the Earth's Radiant Energy System Information and Data, available at: http://ceres.larc.nasa.gov/ (last access: 28 August 2015), NASA, Langley Research Center, Hampton, VA, USA, 2014.

Cleverly, J., Boulain, N., Villalobos-Vega, R., Grant, N., Faux, R., Wood, C., Cook, P. G., Yu, Q., Leigh, A., and Eamus, D.: Dynamics of component carbon fluxes in a semi-arid Acacia woodland, central Australia, J. Geophys. Res.-Biogeo., 118, 1168–1185, doi:10.1002/jgrg.20101, 2013.

Cleverly, J., Eamus, D., Van Gorsel, E., Chen, C., Rumman, R., Luo, Q., Restrepo Coupe, N., Li, L., Kliun, N., Faux, R., Yu, Q., and Huete, A.: Productivity and evapotranspiration of two contrasting semiarid ecosystems following the 2011 carbon land sink anomaly, Agr. Forest Meteorol., under review, 2015.

Collatz, G. J., Ball, J. T., Grivet, C., and Berry, J. A.: Physiological and environmental regulation of stomatal conductance, photosynthesis and transpiration: a model that includes a laminar boundary layer, Agr. Forest Meteorol., 54, 107–136, doi:10.1016/0168-1923(91)90002-8, 1991.

Eamus, D., Hatton, T., Cook, P., and Colvin, C.: Ecohydrology: vegetation function, water and resource management, CSIRO Publishing, Collingwood, VIC, 3066, 2006.

Eamus, D., Cleverly, J., Boulain, N., Grant, N., Faux, R., and Villalobos-Vega, R.: Carbon and water fluxes in an arid-zone Acacia savanna woodland: an analyses of seasonal patterns and responses to rainfall events, Agr. Forest Meteorol., 182–183, 225–238, doi:10.1016/j.agrformet.2013.04.020, 2013.

Ehleringer, J. R., Cerling, T. E., and Helliker, B. R.: C_4 photosynthesis, atmospheric CO_2, and climate, Oecologia, 112, 285–299, 1997.

Falge, E., Baldocchi, D., Olson, R., Anthoni, P., Aubinet, M., Bernhofer, C., Burba, G., Ceulemans, R., Clement, R., Dolman, H., Granier, A., Gross, P., Grünwald, T., Hollinger, D., Jensen, N.-O., Katul, G., Keronen, P., Kowalski, A., Ta Lai, C., Law, B. E., Meyers, T., Moncrieff, J., Moors, E., William Munger, J., Pilegaard, K., Rannik, Ü., Rebmann, C., Suyker, A., Tenhunen, J., Tu, K., Verma, S., Vesala, T., Wilson, K., and Wofsy, S.: Gap filling strategies for long term energy flux data sets, Agr. Forest Meteorol., 107, 71–77, doi:10.1016/S0168-1923(00)00235-5, 2001.

Fasullo, J. T., Boening, C., Landerer, F. W., and Nerem, R. S.: Australia's unique influence on global sea level in 2010–2011, Geophys. Res. Lett., 40, 4368–4373, doi:10.1002/grl.50834, 2013.

Gamon, J. A., Huemmrich, K. F., Stone, R. S., and Tweedie, C. E.: Spatial and temporal variation in primary productivity (NDVI) of coastal Alaskan tundra: decreased vegetation growth following earlier snowmelt, Remote Sens. Environ., 129, 144–153, doi:10.1016/j.rse.2012.10.030, 2013.

Gao, X., Huete, A. R., Ni, W., and Miura, T.: Optical–biophysical relationships of vegetation spectra without background contamination, Remote Sens. Environ., 74, 609–620, doi:10.1016/S0034-4257(00)00150-4, 2000.

Gesch, D. B., Verdin, K. L., and Greenlee, S. K.: New land surface digital elevation model covers the Earth, EOS T. Am. Geophys. Un., 80, 69–70, doi:10.1029/99EO00050, 1999.

Hill, M. J., Held, A. A., Leuning, R., Coops, N. C., Hughes, D., and Cleugh, H. A.: MODIS spectral signals at a flux tower site: relationships with high-resolution data, and CO_2 flux and light use efficiency measurements, Remote Sens. Environ., 103, 351–368, doi:10.1016/j.rse.2005.06.015, 2006.

Huete, A., Justice, C., and Liu, H.: Development of vegetation and soil indices for MODIS-EOS, Remote Sens. Environ., 49, 224–234, doi:10.1016/0034-4257(94)90018-3, 1994.

Huete, A., Didan, K., Miura, T., Rodriguez, E. P., Gao, X., and Ferreira, L. G.: Overview of the radiometric and biophysical performance of the MODIS vegetation indices, Remote Sens. Environ., 83, 195–213, doi:10.1016/S0034-4257(02)00096-2, 2002.

Huete, A., Restrepo-Coupe, N., Ratana, P., Didan, K., Saleska, S., Ichii, K., Panuthai, S., and Gamo, M.: Multiple site tower flux and remote sensing comparisons of tropical forest dynamics in Monsoon Asia, Agr. Forest Meteorol., 148, 748–760, doi:10.1016/j.agrformet.2008.01.012, 2008.

Huete, A. R.: A soil-adjusted vegetation index (SAVI), Remote Sens. Environ., 25, 295–309, doi:10.1016/0034-4257(88)90106-X, 1988.

Huete, A. R. and Tucker, C. J.: Investigation of soil influences in AVHRR red and near-infrared vegetation index imagery, Int. J. Remote Sens., 12, 1223–1242, doi:10.1080/01431169108929723, 1991.

Huete, A. R., Didan, K., Shimabukuro, Y. E., Ratana, P., Saleska, S. R., Hutyra, L. R., Yang, W., Nemani, R. R., and Myneni, R.: Amazon rainforests green-up with sunlight in dry season, Geophys. Res. Lett., 33, L06405, doi:10.1029/2005GL025583, 2006.

Huffman, G. J., Bolvin, D. T., Nelkin, E. J., Wolff, D. B., Adler, R. F., Gu, G., Hong, Y., Bowman, K. P., and Stocker, E. F.: The TRMM Multisatellite Precipitation Analysis (TMPA): quasi-global, multiyear, combined-sensor precipitation estimates at fine scales, J. Hydrometeorol., 8, 38–55, doi:10.1175/JHM560.1, 2007.

Hutley, L. B., O'Grady, A. P., and Eamus, D.: Evapotranspiration from Eucalypt open-forest savanna of northern Australia, Funct. Ecol., 14, 183–194, doi:10.1046/j.1365-2435.2000.00416.x, 2000.

Hutley, L. B., Beringer, J., Isaac, P. R., Hacker, J. M., and Cernusak, L. A.: A sub-continental scale living laboratory: spatial patterns of savanna vegetation over a rainfall gradient in northern Australia, Agr. Forest Meteorol., 151, 1417–1428, doi:10.1016/j.agrformet.2011.03.002, 2011.

Hutyra, L. R., Munger, J. W., Saleska, S. R., Gottlieb, E., Daube, B. C., Dunn, A. L., Amaral, D. F., de Camargo, P. B., and Wofsy, S. C.: Seasonal controls on the exchange of carbon and water in an Amazonian rain forest, J. Geophys. Res.-Biogeo., 112, G03008, doi:10.1029/2006JG000365, 2007.

Isaac, P., Cleverly, J., Beringer, J., and McHugh, I.: The OzFlux network data path: from collection to curation, Biogeosciences, in this issue, 2015.

Johnson, K. A. and Goody, R. S.: The original Michaelis constant: translation of the 1913 Michaelis–Menten paper, Biochemistry, 50, 8264–8269, doi:10.1021/bi201284u, 2011.

Kanniah, K. D., Beringer, J., Hutley, L. B., Tapper, N. J., and Zhu, X.: Evaluation of Collections 4 and 5 of the MODIS gross primary productivity product and algorithm improvement at a tropical savanna site in northern Australia, Remote Sens. Environ., 113, 1808–1822, doi:10.1016/j.rse.2009.04.013, 2009.

Kanniah, K. D., Beringer, J., and Hutley, L. B.: Environmental controls on the spatial variability of savanna productivity in the Northern Territory, Australia, Agr. Forest Meteorol., 151, 1429–1439, doi:10.1016/j.agrformet.2011.06.009, 2011.

Kanniah, K. D., Beringer, J., North, P., and Hutley, L.: Control of atmospheric particles on diffuse radiation and terrestrial plant productivity – a review, Prog. Phys. Geog., 36, 209–237, doi:10.1177/0309133311434244, 2012.

Kanniah, K. D., Beringer, J., and Hutley, L.: Exploring the link between clouds, radiation, and canopy productivity of tropical savannas, Agr. Forest Meteorol., 182–183, 304–313, doi:10.1016/j.agrformet.2013.06.010, 2013.

Kato, S., Loeb, N. G., Rose, F. G., Doelling, D. R., Rutan, D. A., Caldwell, T. E., Yu, L., and Weller, R. A.: Surface irradiances consistent with CERES-derived top-of-atmosphere shortwave and longwave irradiances, J. Climate, 26, 2719–2740, doi:10.1175/JCLI-D-12-00436.1, 2012.

Knyazikhin, Y., Glassy, J., Privette, J. L., Tian, Y., Lotsch, A., Zhang, Y., Wang, Y., Morisette, J. T., Votava, P., Myneni, R. B., Nemani, R. R., and Running, S. W.: MODIS Leaf Area Index (LAI) and Fraction of Photosynthetically Active Radiation Absorbed by Vegetation (FPAR) product (MOD15): algorithm theoretical basis document, available at: http://modis.gsfc.nasa.gov/data/atbd/atbd_mod15.pdf (last access: 20 December 2012), NASA, Earth Observing System Group, Greenbelt, MD, USA, 1999.

Koerber, G. R., Cleverly, J., Isaac, P., and Meyer, W. S.: Use of light-use efficiency functions to describe CO_2 uptake at a semi-arid site, role of leaf-area index and leaf density, methods of estimating ecosystem respiration using LUE curves, Biogeosciences, in this issue, 2015.

Kottek, M., Grieser, J., Beck, C., Rudolf, B., and Rubel, F.: World map of the Köppen–Geiger climate classification updated, Meteorol. Z., 15, 259–263, doi:10.1127/0941-2948/2006/0130, 2006.

Leuning, R., Cleugh, H. A., Zegelin, S. J., and Hughes, D.: Carbon and water fluxes over a temperate *Eucalyptus* forest and a tropical wet/dry savanna in Australia: measurements and comparison with MODIS remote sensing estimates, Agr. Forest Meteorol., 129, 151–173, doi:10.1016/j.agrformet.2004.12.004, 2005.

Ma, X., Huete, A., Yu, Q., Coupe, N. R., Davies, K., Broich, M., Ratana, P., Beringer, J., Hutley, L. B., Cleverly, J., Boulain, N., and Eamus, D.: Spatial patterns and temporal dynamics in savanna vegetation phenology across the North Australian Tropical Transect, Remote Sens. Environ., 139, 97–115, doi:10.1016/j.rse.2013.07.030, 2013.

Ma, X., Huete, A., Yu, Q., Restrepo-Coupe, N., Beringer, J., Hutley, L. B., Kanniah, K. D., Cleverly, J., and Eamus, D.: Parameterization of an ecosystem light-use-efficiency model for predicting savanna GPP using MODIS EVI, Remote Sens. Environ., 154, 253–271, doi:10.1016/j.rse.2014.08.025, 2014.

Maeda, E. E., Heiskanen, J., Aragão, L. E. O. C., and Rinne, J.: Can MODIS EVI monitor ecosystem productivity in the Amazon rainforest?, Geophys. Res. Lett., 41, 2014GL061535, doi:10.1002/2014GL061535, 2014.

Mahadevan, P., Wofsy, S. C., Matross, D. M., Xiao, X., Dunn, A. L., Lin, J. C., Gerbig, C., Munger, J. W., Chow, V. Y., and Gottlieb, E. W.: A satellite-based biosphere parameterization for net ecosystem CO_2 exchange: Vegetation Photosynthesis and Respiration Model (VPRM), Global Biogeochem. Cy., 22, B2005, doi:10.1029/2006GB002735, 2008.

Meyer, W. S., Kondrlovà, E., and Koerber, G. R.: Evaporation of perennial semi-arid woodland in southeastern Australia is adapted for irregular but common dry periods, Hydrol. Process., 29, 3714–3726, doi:10.1002/hyp.10467, 2015.

Michaelis, L. and Menten, M. L.: Die Kinetik der Invertinwirkung, Biochemistry, 49, 333–369, 1913.

Olofsson, P., Lagergren, F., Lindroth, A., Lindström, J., Klemedtsson, L., Kutsch, W., and Eklundh, L.: Towards operational remote sensing of forest carbon balance across Northern Europe, Biogeosciences, 5, 817–832, doi:10.5194/bg-5-817-2008, 2008.

Papaioannou, G., Papanikolaou, N., and Retalis, D.: Relationships of photosynthetically active radiation and shortwave irradiance, Theor. Appl. Climatol., 48, 23–27, doi:10.1007/BF00864910, 1993.

Papale, D., Reichstein, M., Aubinet, M., Canfora, E., Bernhofer, C., Kutsch, W., Longdoz, B., Rambal, S., Valentini, R., Vesala, T., and Yakir, D.: Towards a standardized processing of Net Ecosystem Exchange measured with eddy covariance technique: algorithms and uncertainty estimation, Biogeosciences, 3, 571–583, doi:10.5194/bg-3-571-2006, 2006.

Peng, Y. and Gitelson, A. A.: Remote estimation of gross primary productivity in soybean and maize based on total crop chlorophyll content, Remote Sens. Environ., 117, 440–448, doi:10.1016/j.rse.2011.10.021, 2012.

Poulter, B., Frank, D., Ciais, P., Myneni, R. B., Andela, N., Bi, J., Broquet, G., Canadell, J. G., Chevallier, F., Liu, Y. Y., Running, S. W., Sitch, S., and van der Werf, G. R.: Contribution of semi-arid ecosystems to interannual variability of the global carbon cycle, Nature, 509, 600–603, doi:10.1038/nature13376, 2014.

Restrepo-Coupe, N., Rocha, H. R. da, Christoffersen, B., Araujo, A. C. da, Borma, L. S., Cabral, O. M. R., Camargo, P. B. de, Cardoso, F. L., Costa, A. C. L. da, Fitzjarrald, D. R., Goulden, M. L., Hutyra, L. R., Kruijt, B., Maia, J. M. F., Malhi, Y. S., Manzi, A. O., Miller, S. D., Nobre, A. D., Randow, C. von, Sá, L. D. da A., Sakai, R. K., Tota, J., Wofsy, S. C., Zanchi, F. B., and Saleska, S. R.: What drives the seasonality of productivity across the Amazon basin? A cross-site analysis of eddy flux tower measurements from the Brasil flux network, Agr. Forest Meteorol., 182–183, 128–144, 2013.

Richardson, A. D. and Hollinger, D. Y.: Statistical modeling of ecosystem respiration using eddy covariance data: maximum likelihood parameter estimation, and Monte Carlo simulation of model and parameter uncertainty, applied to three simple models, Agr. Forest Meteorol., 131, 191–208, doi:10.1016/j.agrformet.2005.05.008, 2005.

Rubel, F. and Kottek, M.: Observed and projected climate shifts 1901–2100 depicted by world maps of the Köppen–Geiger climate classification, Meteorol. Z., 19, 135–141, doi:10.1127/0941-2948/2010/0430, 2010.

Running, S. W., Justice, C. O., Salomonson, V., Hall, D., Barker, J., Kaufmann, Y. J., Strahler, A. H., Huete, A. R., Muller, J.-P., Vanderbildt, V., Wan, Z. M., Teillet, P., and Carneggie, D.: Terrestrial remote sensing science and algorithms planned for EOS/MODIS, Int. J. Remote Sens., 15, 3587–3620, doi:10.1080/01431169408954346, 1994.

Running, S. W., Thornton, P. E., Nemani, R., and Glassy, J. M.: Global terrestrial gross and net primary productivity from the Earth Observing System, in: Methods in Ecosystem Science, Springer New York, USA, 44–57, 2000.

Santin-Janin, H., Garel, M., Chapuis, J.-L., and Pontier, D.: Assessing the performance of NDVI as a proxy for plant biomass using non-linear models: a case study on the Kerguelen archipelago, Polar Biol., 32, 861–871, doi:10.1007/s00300-009-0586-5, 2009.

Schaaf, C. B., Gao, F., Strahler, A. H., Lucht, W., Li, X., Tsang, T., Strugnell, N. C., Zhang, X., Jin, Y., Muller, J.-P., Lewis, P., Barnsley, M., Hobson, P., Disney, M., Roberts, G., Dunderdale, M., Doll, C., d'Entremont, R. P., Hu, B., Liang, S., Privette, J. L., and Roy, D.: First operational BRDF, albedo nadir reflectance products from MODIS, Remote Sens. Environ., 83, 135–148, doi:10.1016/S0034-4257(02)00091-3, 2002.

Shen, S. and Leptoukh, G. G.: Estimation of surface air temperature over central and eastern Eurasia from MODIS land surface temperature, Environ. Res. Lett., 6, 045206, doi:10.1088/1748-9326/6/4/045206, 2011.

Sims, D. A., Rahman, A. F., Cordova, V. D., El-Masri, B. Z., Baldocchi, D. D., Flanagan, L. B., Goldstein, A. H., Hollinger, D. Y., Misson, L., Monson, R. K., Oechel, W. C., Schmid, H. P., Wofsy, S. C., and Xu, L.: On the use of MODIS EVI to assess gross primary productivity of

North American ecosystems, J. Geophys. Res., 111, G04015, doi:10.1029/2006JG000162, 2006.

Sims, D. A., Rahman, A. F., Cordova, V. D., El-Masri, B. Z., Baldocchi, D. D., Bolstad, P. V., Flanagan, L. B., Goldstein, A. H., Hollinger, D. Y., Misson, L., Monson, R. K., Oechel, W. C., Schmid, H. P., Wofsy, S. C., and Xu, L.: A new model of gross primary productivity for North American ecosystems based solely on the enhanced vegetation index and land surface temperature from MODIS, Remote Sens. Environ., 112, 1633–1646, doi:10.1016/j.rse.2007.08.004, 2008.

Sjöström, M., Ardö, J., Arneth, A., Boulain, N., Cappelaere, B., Eklundh, L., de Grandcourt, A., Kutsch, W. L., Merbold, L., Nouvellon, Y., Scholes, R. J., Schubert, P., Seaquist, J., and Veenendaal, E. M.: Exploring the potential of MODIS EVI for modeling gross primary production across African ecosystems, Remote Sens. Environ., 115, 1081–1089, doi:10.1016/j.rse.2010.12.013, 2011.

Stoy, P. C., Katul, G. G., Siqueira, M. B. S., Juang, J.-Y., Novick, K. A., Uebelherr, J. M., and Oren, R.: An evaluation of models for partitioning eddy covariance-measured net ecosystem exchange into photosynthesis and respiration, Agr. Forest Meteorol., 141, 2–18, doi:10.1016/j.agrformet.2006.09.001, 2006.

Suyker, A. E. and Verma, S. B.: Year-round observations of the net ecosystem exchange of carbon dioxide in a native tallgrass prairie, Glob. Change Biol., 7, 279–289, doi:10.1046/j.1365-2486.2001.00407.x, 2001.

Szeicz, G.: Solar radiation for plant growth, J. Appl. Ecol., 11, 617–636, 1974.

Taylor, K. E.: Summarizing multiple aspects of model performance in a single diagram, J. Geophys. Res., 106, 7183–7192, doi:10.1029/2000JD900719, 2001.

Tezara, W., Mitchell, V. J., Driscoll, S. D., and Lawlor, D. W.: Water stress inhibits plant photosynthesis by decreasing coupling factor and ATP, Nature, 401, 914–917, doi:10.1038/44842, 1999.

TRMM: Tropical Rainfall Measuring Mission Project, 3B43: Monthly 0.25 × 0.25 merged TRMM and other estimates v7, NASA Distrib. Active Arch. Cent., NASA, Goddard Space Flight Cent. Earth Sci., Greenbelt, MD, USA, available at: http://mirador.gsfc.nasa.gov/collections/TRMM_3B43_007.shtml (last access: 27 February 2014), 2014.

Van Gorsel, E.: Impact of the 2012–2013 summer heat records on forest productivity in eastern Australia, Biogeosciences, 2015.

Van Gorsel, E., Berni, J. A. J., Briggs, P., Cabello-Leblic, A., Chasmer, L., Cleugh, H. A., Hacker, J., Hantson, S., Haverd, V., Hughes, D., Hopkinson, C., Keith, H., Kljun, N., Leuning, R., Yebra, M., and Zegelin, S.: Primary and secondary effects of climate variability on net ecosystem carbon exchange in an evergreen *Eucalyptus* forest, Agr. Forest Meteorol., 182–183, 248–256, doi:10.1016/j.agrformet.2013.04.027, 2013.

van Niel, T. G., McVicar, T. R., Roderick, M. L., van Dijk, A. I. J. M., Beringer, J., Hutley, L. B., and van Gorsel, E.: Upscaling latent heat flux for thermal remote sensing studies: comparison of alternative approaches and correction of bias, J. Hydrol., 468–469, 35–46, doi:10.1016/j.jhydrol.2012.08.005, 2012.

Veroustraete, F., Sabbe, H., and Eerens, H.: Estimation of carbon mass fluxes over Europe using the C-Fix model and Euroflux data, Remote Sens. Environ., 83, 376–399, doi:10.1016/S0034-4257(02)00043-3, 2002.

Vitasse, Y., Lenz, A., and Körner, C.: The interaction between freezing tolerance and phenology in temperate deciduous trees, Front Plant Sci., 5, 00541, doi:10.3389/fpls.2014.00541, 2014.

Wang, J., Rich, P. M., Price, K. P., and Kettle, W. D.: Relations between NDVI and tree productivity in the central Great Plains, Int. J. Remote Sens., 25, 3127–3138, doi:10.1080/0143116032000160499, 2004.

Waring, H. R. and Running, W. S.: Forest Ecosystems: Analysis at Multiple Scales, Academic Press, San Diego, CA, USA, 1998.

Wofsy, S., Goulden, M., and Munger, J. W.: Net exchange of CO_2 in a mid-latitude forest, Science, 260, 1314–1317, 1993.

Wu, C., Niu, Z., and Gao, S.: Gross primary production estimation from MODIS data with vegetation index and photosynthetically active radiation in maize, J. Geophys. Res., 115, D12127, doi:10.1029/2009JD013023, 2010.

Wu, C., Chen, J. M., and Huang, N.: Predicting gross primary production from the enhanced vegetation index and photosynthetically active radiation: evaluation and calibration, Remote Sens. Environ., 115, 3424–3435, doi:10.1016/j.rse.2011.08.006, 2011.

Xiao, X., Zhang, Q., Braswell, B., Urbanski, S., Boles, S., Wofsy, S., Moore III, B., and Ojima, D.: Modeling gross primary production of temperate deciduous broadleaf forest using satellite images and climate data, Remote Sens. Environ., 91, 256–270, doi:10.1016/j.rse.2004.03.010, 2004.

Zolfaghar, S.: Comparative ecophysiology of *Eucalyptus* woodlands along a depth-to-groundwater gradient, PhD thesis, University Technology of Sydney, Sydney, Australia, 1 September, 2013.

Table 1. OzFlux sites presented in this study-location and additional information.

ID	Site name	Measurement period		Elevation	Lat	Lon	Vegetation height	Biome	u^*_{tresh}	u^*_{tresh} min	u^*_{tresh} max
		Start	End	(m)	(deg)	(deg)	(m)		(m s^{-1})	(m s^{-1})	(m s^{-1})
HSP	Howard Springs	2001	2011	64	−12.495	131.150	15	Open woodland savanna	0.124	0.000	0.255
ASP	Alice Springs Mulga	2010	2013	606	−22.283	133.249	6	*Acacia* Mulga	0.105	0.000	0.215
TBR	Tumbarumba	2001	2011	1200	−35.657	148.152	40	Wet sclerophyll forest	0.230	0.000	0.505
CHO	Calperum–Chowilla	2010	2012	379	−34.003	140.588	5	Malle	0.176	0.086	0.265

Table 2. Remote sensing data sources, cell size, sample size (eddy-covariance tower-site at the centre pixel) and time interval.

MODIS product	Description	Data Source	Cell Size	Sample Size	Interval
LAI_{MOD}	Leaf Area Index	MOD15A2	1000 m	1 × 1	8 Day
$fPAR_{MOD}$	Fraction of Absorbed PAR	MOD15A2	1000 m	1 × 1	8 Day
LST_{day}	Daytime Land Surface Temperature	MOD11A2	1000 m	1 × 1	8 Day
GPP_{MOD}	Gross Primary Production	MOD17A2	1000 m	1 × 1	8 Day
EVI_{SZA30}	NBAR Enhanced Vegetation Index	MCD43A1	500 m	2 × 2	8 Day
$NDVI_{SZA30}$	NBAR Normalized Difference Vegetation Index	MCD43A1	500 m	2 × 2	8 Day

Table 3. Linear regressions obtained by a nonlinear mixed-effects regression model for gross ecosystem productivity (GEP, $\mathrm{gC\,m^{-2}\,d^{-1}}$) vs. combinations of 16-day average MODIS products: fixed solar zenith angle of 30° enhanced vegetation index ($\mathrm{EVI_{SZA30}}$), daytime and Land Surface Temperature ($\mathrm{LST_{day}}$, °C), fixed solar zenith angle of 30° normalized difference vegetation index ($\mathrm{NDVI_{SZA30}}$), precipitation from the Tropical Rainfall Measuring Mission ($\mathrm{Precip_{TRMM}}$, $\mathrm{mm\,month^{-1}}$) data product from 1998–2013 (TR<<, 2014; $\mathrm{mm\,month^{-1}}$), and surface shortwave incident radiation from the Clouds and the Earth's Radiant Energy System ($\mathrm{SW_{CERES}}$, $\mathrm{W\,m^{-2}}$) data product from 2000–2013 (CERES, 2014). Model runs for HSP: Howard Springs, ASP: Alice Springs Mulga, CHO: Calperum–Chowilla, and TBR: Tumbarumba, and all available data (includes all sites). Bold fonts highlight values mentioned on the text.

	HSP				ASP				TMB			
	Coeff [*a b c d*]	CI	R^2	AIC	Coeff	CI	R^2	AIC	Coeff	CI	R^2	AIC
$\mathrm{GEP} = a\ \mathrm{EVI}_{\mathrm{SZA30}} + b$	**[21.94 −2.65]**	**[0.96 0.28]**	**0.82**	**263**	**[26.01 −2.48]**	**[1.69 0.2]**	**0.85**	**64**	[15.52 0.90]	[5.55 2.01]	0.03	740
$\mathrm{GEP} = ,a\ \mathrm{NDVI}_{\mathrm{SZA30}}$	[15.03 −4.11]	[0.70 0.35]	0.78	275	[14.34 −3.10]	[0.99 0.26]	0.83	80	[19.05 −7.28]	[5.23 3.79]	0.07	733
$\mathrm{GEP} = a\ \mathrm{LST}_{\mathrm{day}} + b$	[−0.22 70.91]	[0.02 7.70]	0.28	676	[−0.02 7.59]	[0.013 3.90]	0.03	218	**[0.26 −68.09]**	**[0.015 4.45]**	**0.58**	**656**
$\mathrm{GEP} = a\ \mathrm{Precip}_{\mathrm{TRMM}} + b$	[0.01 3.03]	[0.001 0.11]	0.53	627	[0.01 0.38]	[0.004 0.11]	0.30	182	[−0.017 7.54]	[0.005 0.31]	0.03	799
$\mathrm{GEP} = a\ \mathrm{SW}_{\mathrm{CERES}} + b$	[−0.012 7.30]	[0.006 1.48]	0.02	781	[0.005 −0.30]	[0.002 0.59]	0.02	209	[0.026 1.025]	[0.001 0.26]	0.60	635
$\mathrm{GEP} = a\ \mathrm{EVI}_{\mathrm{SZA30}} + b\ \mathrm{LST}_{\mathrm{day}} + c\ \mathrm{LST}_{\mathrm{day}}\mathrm{EVI} + d$	[−29.96 127.38 0.09 −0.34]	[18.42 66.60 0.06 0.22]	0.82	268	[−11.51 76.94 0.03 −0.16]	[7.81 67.35 0.03 0.22]	0.87	66	[−2.64 1.38 0.08]	[0.21 10.71 0.04]	0.64	583
$\mathrm{GEP} = a\ \mathrm{EVI}_{\mathrm{SZA30}} + b\ \mathrm{SW}_{\mathrm{CERES}} + c\ \mathrm{SW}_{\mathrm{CERES}}\mathrm{EVI} + d$	**[−3.57 24.15 0.003 −0.004]**	**[3.45 11.26 0.01 0.05]**	**0.82**	**266**	[2.48 −21.70 −0.02 0.19]	[0.99 8.68 0.004 0.03]	0.87	54	**[7.75 −19.41 −0.05 0.21]**	**[3.25 8.84 0.017 0.05]**	**0.70**	**553**
$\mathrm{GEP} = a\ \mathrm{SW}_{\mathrm{CERES}} + b\ \mathrm{SW}_{\mathrm{CERES}}\mathrm{EVI}_{\mathrm{SZA30}} + c$	[3.63– 0.03 0.097]	[0.73 0.003 0.004]	0.82	263	**[−0.008 −0.01 0.10]**	**[0.18 0.001 0.006]**	**0.88**	**56**	[0.69 −0.014 0.12]	[0.29 0.006 0.016]	0.69	554
$\mathrm{GEP} = a\ \mathrm{EVI}_{\mathrm{SZA30}} + b\ \mathrm{Precip}_{\mathrm{TRMM}} + c\ \mathrm{Precip}_{\mathrm{TRMM}}\mathrm{EVI}_{\mathrm{SZA30}} + d$	**[−2.13 18.93 0.01 −0.02]**	**[0.34 1.28 0.004 0.01]**	**0.84**	**253**	**[−1.32 15.09 −0.019 0.18]**	**[0.25 2.19 0.005 0.04]**	**0.88**	**42**	[1.63 15.31 0.002 −0.04]	[3.78 10.29 0.06 0.16]	0.04	732
$\mathrm{GEP} = a\ \mathrm{NDVI}_{\mathrm{SZA30}} + b\ \mathrm{LST}_{\mathrm{day}} + c\ \mathrm{LST}_{\mathrm{day}}\mathrm{EVI} + d$	[−57.78 118 0.17 −0.33]	[23.79 48.54 0.08 0.16]	0.79	279	[−24.42 79.28 0.07 −0.21]	[9.19 36 0.03 0.12]	0.86	75	[231 −416.25 −0.83 1.51]	[105.9 145.1 0.37 0.50]	0.68	566
$\mathrm{GEP} = a\ \mathrm{NDVI}_{\mathrm{SZA30}} + b\ \mathrm{SW}_{\mathrm{CERES}} + c\ \mathrm{SW}_{\mathrm{CERES}}\mathrm{NDVI}_{\mathrm{SZA30}} + d$	[−9.6 23.6 0.02 −0.03]	[4.76 9.06 0.02 0.04]	0.79	277	[2.77 −11.51 −0.02 0.10]	[1.38 5.41 0.006 0.02]	0.87	62	**[13.58 −17.68 −0.12 0.198]**	**[6.53 8.95 0.032 0.04]**	**0.71**	**542**
$\mathrm{GEP} = a\ \mathrm{SW}_{\mathrm{CERES}} + b\ \mathrm{SW}_{\mathrm{CERES}}\mathrm{NDVI}_{\mathrm{SZA30}} + c$	[2.63 −0.031 0.07]	[0.79 0.004 0.003]	0.78	277	[−0.15 −0.01 0.06]	[0.19 0.001 0.004]	0.88	64	**[0.72 −0.056 0.11]**	**[0.29 0.01 0.014]**	**0.71**	**542**

Title Page
Abstract Introduction
Conclusions References
Tables Figures
◄ ►
Back Close
Full Screen / Esc
Printer-friendly Version
Interactive Discussion

Table 3. Continued.

	CHO Coeff	CI	R^2	AIC	All Coeff	CI	R^2	AIC
GEP = a EVI$_{\mathrm{SZA30}}$ + b	**[12.74 −0.71]**	**[2.05 0.38]**	**0.36**	**49**	**[22.47 −2.19]**	**[0.51 0.1]**	**0.69**	**1323**
GEP = , a NDVI$_{\mathrm{SZA30}}$	[3.97 0.24]	[1.29 0.46]	0.09	70	**[12.62 −2.74]**	**[0.27 0.12]**	**0.72**	**1276**
GEP = a LST$_{\mathrm{day}}$ + b	[0.017 −3.27]	[0.006 1.74]	0.12	69	[−0.095 32.57]	[0.01 3.13]	0.14	2279
GEP = a Precip$_{\mathrm{TRMM}}$ + b	[0.0006 1.66]	[0.003 0.097]	0.02	73	[0.009 3.60]	[0.001 0.14]	0.13	2340
GEP = a SW$_{\mathrm{CERES}}$ + b	[0.003 1.14]	[0.0008 0.14]	0.12	67	[0.007 2.81]	[0.0016 0.32]	0.01	2329
GEP = a EVI$_{\mathrm{SZA30}}$ + b LST$_{\mathrm{day}}$ + c LST$_{\mathrm{day}}$EVI + d	**[22.6 −145.8 −0.08 0.53]**	**[9.4 51.44 0.03 0.17]**	**0.63**	**30**	[−5.60 17.51 0.01 0.02]	[2.98 13.87 0.01 0.05]	0.70	1322
GEP = a EVI$_{\mathrm{SZA30}}$ + b SW$_{\mathrm{CERES}}$ + c SW$_{\mathrm{CERES}}$EVI + d	**[1.87 −4.52 −0.01 0.095]**	**[0.83 4.41 0.005 0.025]**	**0.62**	**26**	**[−0.31 4.95 −0.009 0.079]**	**[0.35 1.45 0.001 0.007]**	**0.82**	**1154**
GEP = a SW$_{\mathrm{CERES}}$ + b SW$_{\mathrm{CERES}}$EVI$_{\mathrm{SZA30}}$ + c	**[1.023 −0.01 0.07]**	**[0.097 0.001 0.008]**	**0.62**	**23**	[0.92 −0.014 0.1]	[0.13 0.001 0.002]	0.82	1179
GEP = a EVI$_{\mathrm{SZA30}}$ + b Precip$_{\mathrm{TRMM}}$ + c Precip$_{\mathrm{TRMM}}$EVI$_{\mathrm{SZA30}}$ + d	[0.21 6.96 −0.03 0.2]	[0.69 3.57 0.015 0.08]	0.52	43	[−2.35 22.48 0.008 −0.02]	[0.14 0.64 0.003 0.009]	0.66	1312
GEP = a NDVI$_{\mathrm{SZA30}}$ + b LST$_{\mathrm{day}}$ + c LST$_{\mathrm{day}}$EVI + d	**[34.5 −119.1 −0.12 0.43]**	**[10.8 29.76 0.036 0.1]**	**0.60**	**34**	[0.43 −27.31 −0.01 0.14]	[3.17 7.05 0.01 0.024]	0.79	1226
GEP = a NDVI$_{\mathrm{SZA30}}$ + b SW$_{\mathrm{CERES}}$ + c SW$_{\mathrm{CERES}}$NDVI$_{\mathrm{SZA30}}$ + d	**[2.74 −5.59 −0.02 0.07]**	**[0.88 2.32 0.005 0.014]**	**0.60**	**30**	**[−0.75 2.8 −0.01 0.05]**	**[0.37 0.75 0.001 0.003]**	**0.88**	**1013**
GEP = a SW$_{\mathrm{CERES}}$ + b SW$_{\mathrm{CERES}}$NDVI$_{\mathrm{SZA30}}$ + c	[0.69 −0.01 0.04]	[0.12 0.002 0.005]	0.57	30	[0.64 −0.016 0.058]	[0.12 0.0006 0.001]	0.87	1052

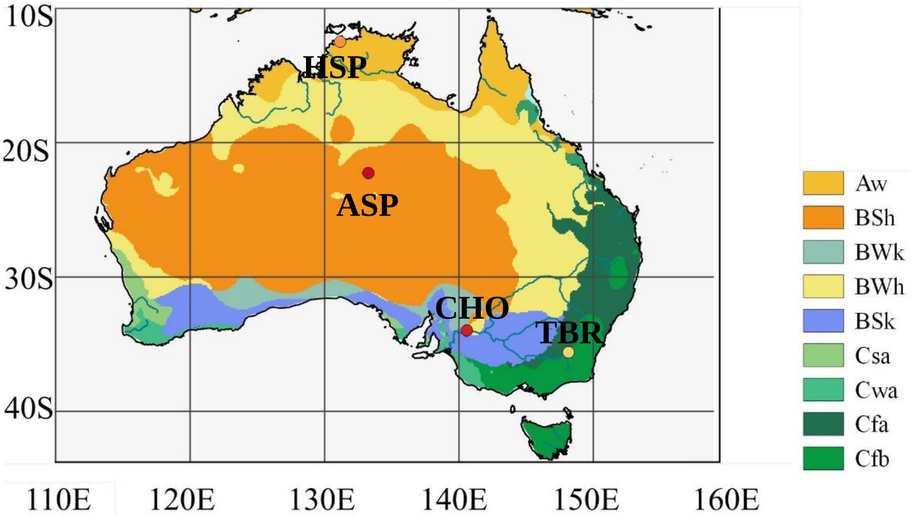

Figure 1. Location of four OzFlux eddy covariance tower sites included on this analysis: HSP: Howard Springs (at Aw), ASP: Alice Springs Mulga (at boundary BSh and BWh), CHO: Calperum-Chowilla (at Bwk), and TBR: Tumbarumba (at boundary Cfa and Cfb). Köppen-Geiger climate classification as published by Kottek et al. (2006) and Rubel and Kottek (2010). Where Aw is equatorial winter dry climate, BSh is arid steppe, BWh is hot arid desert, BWk is cold arid desert, Cfb is warm temperate fully humid warm summer, Cfa is warm temperate fully humid hot summer and Cwa is warm temperate winter dry hot summer.

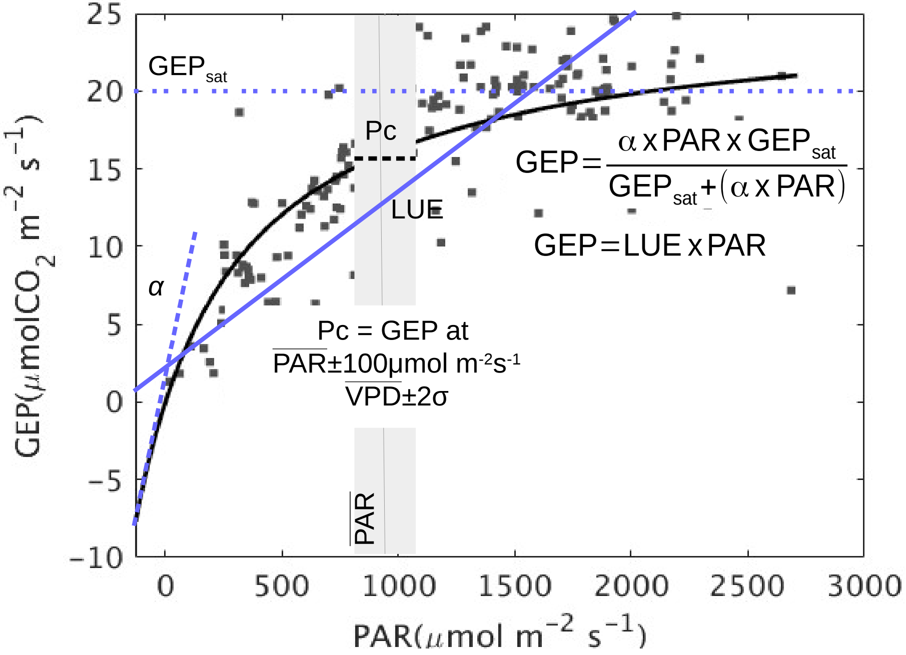

Figure 2. Rectangular hyperbola fitted to 16-day worth of hourly gross ecosystem productivity (GEP, µmol CO$_2$ m^{-2} s^{-1}) versus photosynthetic active radiation (PAR, µmol m^{-2} s^{-1}) data measured at Howard Springs eddy covariance tower (black line). From the rectangular hyperbola: quantum yield (α, µmol CO$_2$ µmol^{-1}; blue dashed line) and GEP at saturation (GEP-sat, µmol CO$_2$ m^{-2} s^{-1}; blue doted line). Photosynthetic capacity (Pc, µCO$_2$ m^{-2} s^{-1}; black dashed line) was calculated as the 16-day mean GEP at mean annual daytime PAR ($\overline{\text{PAR}}$) ±100 µmol m^{-2} s^{-1} (grey area) and mean annual VPD ($\overline{\text{VPD}}$) ±2 standard deviations. Light use efficiency (LUE, µmol CO$_2$ µmol^{-1}) was defined as the ratio between daily GEP over PAR, the slope of the linear regression (blue line).

Title Page
Abstract
Introduction
Conclusions
References
Tables
Figures
◀
▶
Back
Close
Full Screen / Esc
Printer-friendly Version
Interactive Discussion

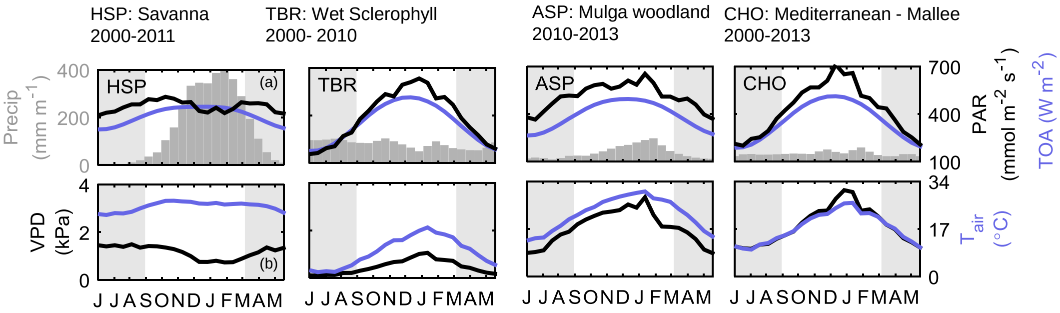

Figure 3. Savanna (HSP), wet sclerophyll (TBR), Mulga (ASP), and Mallee (CHO) ecosystems, OzFlux sites annual cycle (16-day composites) of **(a)** precipitation (Precip; mm month^{-1}; grey bars) and photosynthetic active radiation (PAR; µmol m^{-2} d^{-1}; blue line), and **(b)** vapour pressure deficit (VPD; kPa; black line) and air temperature (T_{air}; °C; blue line). Grey boxes indicate Southern Hemisphere spring and summer September to March.

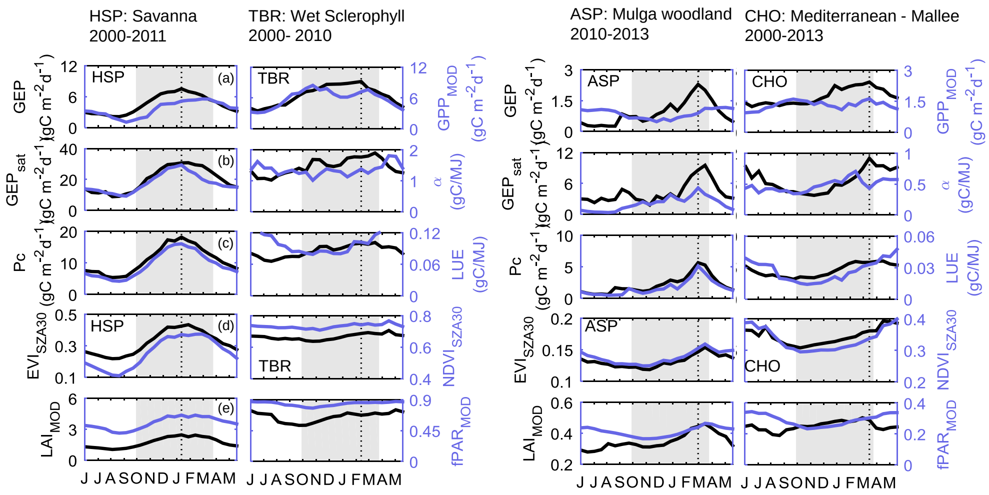

Figure 4. Savana (HSP), wet sclerophyll (TBR), Mulga (ASP), and Mallee (CHO) ecosystems, OzFlux sites annual cycle (16-day composites) of eddy flux derived **(a)** Gross Ecosystem Productivity (GEP; $\mathrm{g\,C\,m^{-2}\,d^{-1}}$; black line) and MODIS Gross Primary Productivity ($\mathrm{GPP_{MOD}}$) product (light blue line); **(b)** GEP at saturation light ($\mathrm{GEP_{sat}}$; $\mathrm{g\,C\,m^{-2}\,d^{-1}}$; black line) and ecosystem quantum yield (α; $\mathrm{g\,C\,MJ^{-1}}$; light blue line); **(c)** photosynthetic capacity (Pc; $\mathrm{g\,C\,m^{-2}\,d^{-1}}$; black line) and the ratio of GEP over PAR (black line), the light use efficiency (LUE; $\mathrm{g\,C\,MJ^{-1}}$; light blue line). At the bottom two panels, satellite derived data of: **(d)** MODIS Enhanced Vegetation Index at fixed solar zenith angle of 30° ($\mathrm{EVI_{SZA30}}$; black line) and the Normalized Difference Vegetation Index ($\mathrm{NDVI_{SZA30}}$; light blue line); **(e)** MODIS Leaf Area Index ($\mathrm{LAI_{MOD}}$; black line) and MODIS Fraction of the Absorbed Photosynthetic Active Radiation ($\mathrm{fPAR_{MOD}}$; light blue line). Grey boxes indicate Southern Hemisphere spring and summer September to March. Black dashed vertical line indicates the timing of maximum GEP.

Title Page
Abstract | Introduction
Conclusions | References
Tables | Figures
◀| |▶
◀ ▶
Back | Close
Full Screen / Esc
Printer-friendly Version
Interactive Discussion

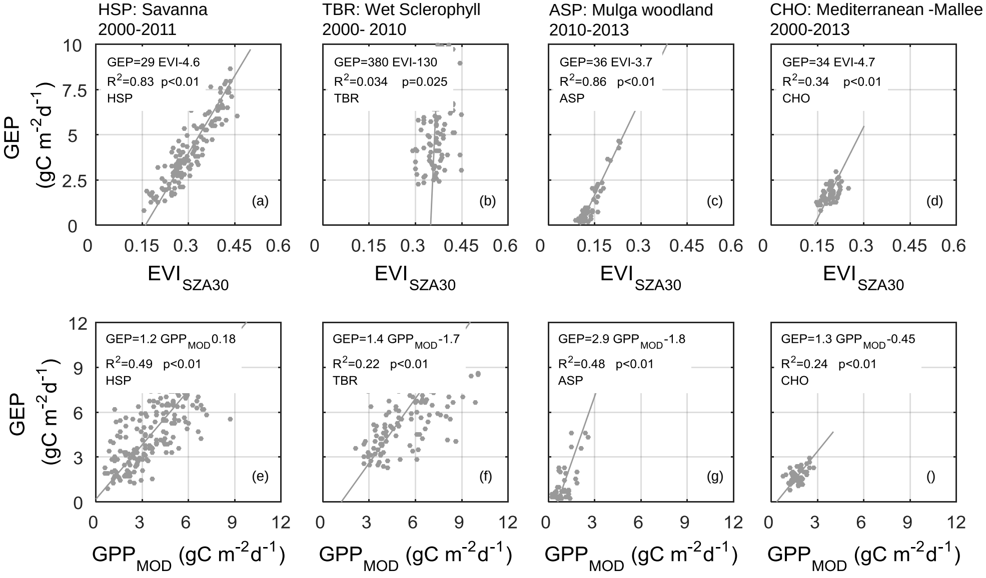

Figure 5. Top row: linear regression between 16 and 8-day time series of measured gross ecosystem productivity (GEP; $\mathrm{g\,C\,m^{-2}\,d^{-1}}$; top row) and the MODIS fixed solar zenith angle of 30° enhanced vegetation index (EVI_{SZA30}) at **(a)** Howard Springs (HSP) open woodland savanna, **(b)** Alice Springs Mulga (ASP), **(c)** Tumbarumba (TBR) wet sclerophyll forest eddy, and **(d)** Chowilla Mallee (CHO) covariance site. Lower row: regression between GEP and MODIS gross primary productivity (GPP_{MOD}) **(e)** HSP, **(f)** TBR, **(g)** ASP, and **(h)** CHO.

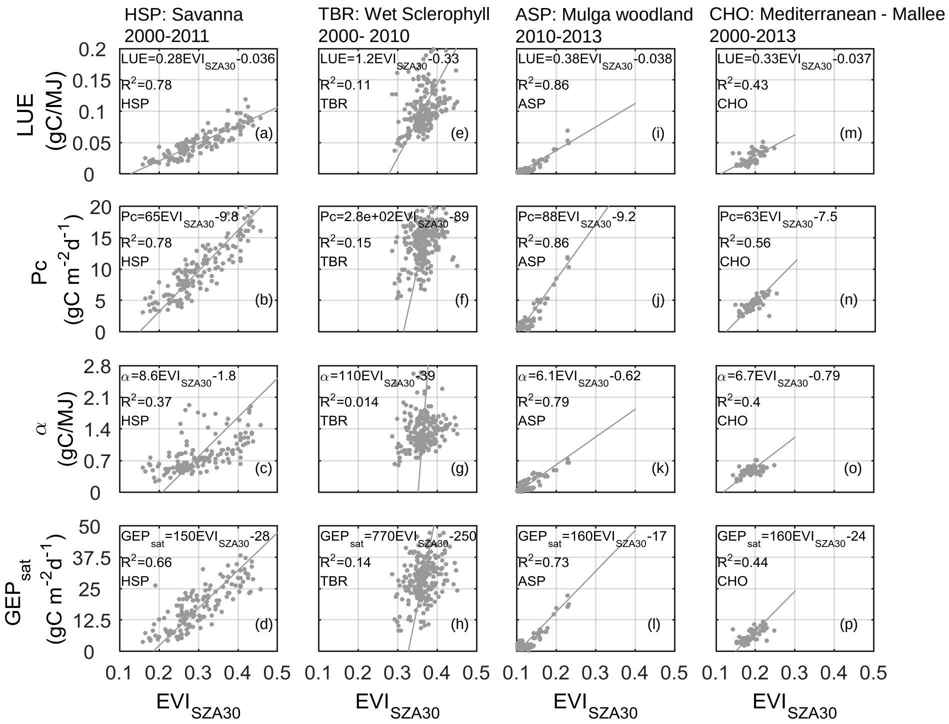

Figure 6. Relationships between 16-day mean values of **(a)** light use efficiency (LUE; $\mathrm{g\,C\,MJ^{-1}}$), **(b)** photosynthetic capacity (Pc; $\mathrm{g\,C\,m^{-2}\,d^{-1}}$), **(c)** ecosystem quantum yield (α; $\mathrm{g\,C\,MJ^{-1}}$), and **(d)** GEP at saturation light ($\mathrm{GEP_{sat}}$; $\mathrm{g\,C\,m^{-2}\,d^{-1}}$), and MODIS fixed solar zenith angle of 30° enhanced vegetation index ($\mathrm{EVI_{SZA30}}$). Four key Australian ecosystem sites, from left to right (columns), HSP savanna, ASP Mulga, wet sclerophyll forest of TBR and CHO Mallee.

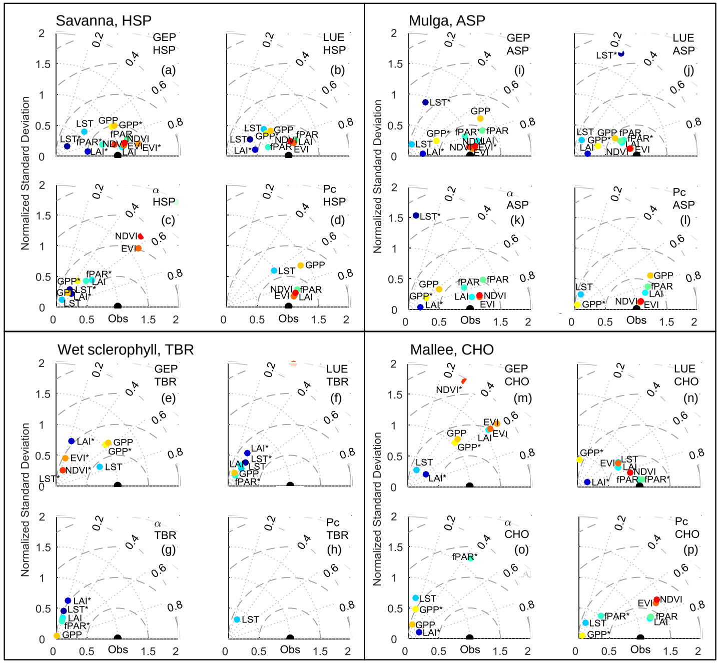

Figure 7. Taylor diagrams showing model results for Howard Springs (HSP), Tumbarumba (TBR), Alice Springs (ASP) and Calperum–Chowilla (CHO) based on site-specific and all sites linear regressions between gross ecosystem productivity (GEP), light use efficiency (LUE), photosynthetic capacity (Pc) and ecosystem quantum yield (α) and different remote sensing products MODIS fixed solar zenith angle of 30° Enhanced Vegetation Index (EVI) and Normalized Difference Vegetation Index (NDVI), Gross Primary Productivity product (GPP), Daytime Land Surface Temperature (LST), Leaf Area Index (LAI), fraction of the absorbed Photosynthetic Active Radiation (fPAR). All site relationships is labelled with an asterisk (e.g. EVI*). EVI and NDVI labels are used instead of $\text{EVI}_{\text{SZA30}}$ and $\text{NDVI}_{\text{SZA30}}$ for displaying purposes. Missing sites indicate that the model overestimates the seasonality of observations – model normalized standard deviation is > 2.

Title Page
Abstract | Introduction
Conclusions | References
Tables | Figures
◀| |▶
◀ ▶
Back | Close
Full Screen / Esc
Printer-friendly Version
Interactive Discussion

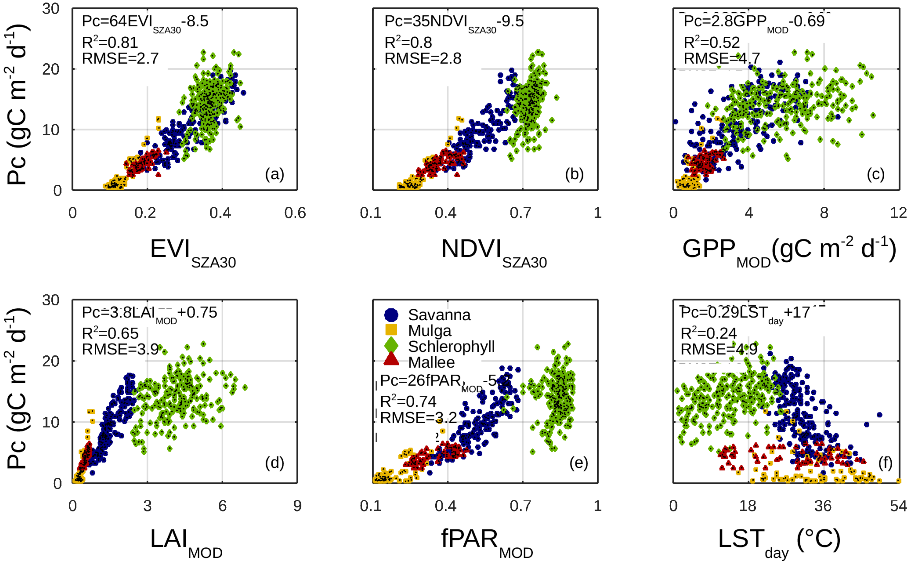

Figure 8. Relationships between 16-day mean values of photosynthetic capacity (Pc; $gC\,m^{-2}\,d^{-1}$) and different RS products: **(a)** MODIS fixed solar zenith angle of 30° enhanced vegetation index (EVI_{SZA30}), **(b)** normalized difference vegetation index ($NDVI_{SZA30}$), **(c)** MODIS gross primary productivity (GPP_{MOD}, $gC\,m^{-2}\,d^{-1}$), **(d)** leaf area index (LAI_{MOD}), **(e)** fraction of the absorbed photosynthetic active radiation ($fPAR_{MOD}$) and **(f)** daytime Land Surface Temperature (LST_{day}, °C). Four key Australian ecosystem sites included on the analysis: HSP savanna (blue circles), ASP Mulga (yellow square markers), CHO Mallee (red triangles) and wet sclerophyll forest of TBR (green diamonds).